


## Research Article

# Synthesis and Characterization of Novel [2 + 1] Tricarbonyl Rhenium Complexes with the Hydrophilic Phosphine Ligands PTA and CAP

Ioanna Roupa,<sup>1</sup> Charalampos Flampouraris,<sup>1</sup> Antonio Shegani,<sup>1</sup> Myrto Ischyropoulou,<sup>1</sup> Konstantina Makrypidi,<sup>1</sup> Catherine Raptopoulou,<sup>2</sup> Ioannis Pirmettis,<sup>1</sup> Minas S. Papadopoulos,<sup>1</sup> Vassilis Psycharis,<sup>2</sup> and Aristeidis Chiotellis<sup>1</sup> 

<sup>1</sup>Institutes of Nuclear & Radiological Sciences & Technology, Energy & Safety, National Center for Scientific Research “Demokritos”, 15310 Athens, Greece

<sup>2</sup>Institutes of Nanoscience and Nanotechnology, National Center for Scientific Research “Demokritos”, 15310 Athens, Greece

Correspondence should be addressed to Aristeidis Chiotellis; [achiotel@rrp.demokritos.gr](mailto:achiotel@rrp.demokritos.gr)

Received 18 February 2022; Revised 5 May 2022; Accepted 18 May 2022; Published 13 June 2022

Academic Editor: Franc Perdih

Copyright © 2022 Ioanna Roupa et al. This is an open access article distributed under the Creative Commons Attribution License, which permits unrestricted use, distribution, and reproduction in any medium, provided the original work is properly cited.

In the pursuit of hydrophilic model  $fac\text{-[Re(CO)}_3\text{)]}^+$  complexes for (radio) pharmaceutical applications, six novel [2 + 1] mixed-ligand complexes of the general type  $fac\text{-[Re(CO)}_3\text{(bid)P]}$  were synthesized and characterized, where bid is a bidentate ligand bearing either (N, O) or (S, S') donor atom sets and P is the hydrophilic phosphine 1,3,5-triaza-7-phosphoadamantane (PTA) or its macrocyclic homologue 1,4,7-triaza-9-phosphatricyclo[5.3.2.1]tridecane (CAP). The (N, O) ligands used in this study were picolinic and quinaldic acid, while the (S, S') ligand was diethyldithiocarbamate. The complexes were synthesized in generally high yields and purity and the characterization was performed by spectroscopic methods, IR, NMR, and elemental analysis. Detailed X-ray crystallographic study of molecular packing by using Hirshfeld analysis tools revealed a plethora of intermolecular interactions such as hydrogen bond,  $\pi\cdots\pi$ , C-H $\cdots\pi$ , and carbonyl-carbonyl interactions. To our knowledge, the CAP complexes reported herein are the first example of [2 + 1] mixed-ligand  $fac\text{-[Re(CO)}_3\text{)]}^+$  complexes with CAP. The new complexes might have the potential to serve as platforms for the design of target-specific complexes with favorable pharmacokinetics.

## 1. Introduction

Rhenium has recently attracted renewed attention in medicine due to its increasing potential applications in the anticancer arena. In fact, two isotopes of rhenium are  $\beta$ -emitters ( $^{186}\text{Re}$ ,  $E_{\max} = 1.1$  MeV,  $t_{1/2} = 90.6$  h;  $^{188}\text{Re}$ ,  $E_{\max} = 2.1$  MeV,  $t_{1/2} = 17$  h) and therefore they are suitable candidates for therapeutic applications in radiotherapy [1]. In addition, rhenium shares a very similar chemistry with  $^{99\text{m}}\text{Tc}$ , the most widely used Single Photon Emission Computed Tomography (SPECT) radioisotope in Nuclear Medicine, and therefore any advancements in synthetic methodologies to access rhenium complexes can be usually applied for the development of more efficient  $^{99\text{m}}\text{Tc}$  radiopharmaceuticals [2]. Furthermore, recent research has

shown that rhenium complexes possess potent anticancer properties while exhibiting diverse mechanisms of action, which makes them promising chemotherapeutic agents [3]. In view of the above, the exploration of rhenium's coordination chemistry remains an important aspect for the development of novel (radio) agents with optimal biological performance.

Increased hydrophilicity is often a central feature of pharmaceutical design because such compounds have favorable *in vivo* characteristics for medical applications [4] (e.g., increased aqueous media solubility and faster clearance of the drug from the body). The organometallic  $fac\text{-[M(CO)}_3\text{)]}^+$  core ( $M = ^{\text{nat}}\text{Re}$ ,  $^{186/188}\text{Re}$  and  $^{99\text{m}}\text{Tc}$ ) is undoubtedly the most versatile precursor for the development of complexes of (radio) pharmaceutical interest. However,

its increased lipophilicity can negatively influence the pharmacokinetic profile of the corresponding complexes [5]. This problem can be further exacerbated when common phosphines are used as ligands despite them being suitable for stabilizing metals in intermediate to low oxidation states as in the *fac*-[M(CO)<sub>3</sub>]<sup>+</sup> core, thanks to their  $\pi$ -acceptor and  $\sigma$ -donor properties [6]. The high lipophilicity and molecular weight of common aryl- and alkyl phosphines usually render these ligands incompatible for target-specific (radio) pharmaceutical applications.

Nevertheless, the hydrophilicity of *fac*-[M(CO)<sub>3</sub>]<sup>+</sup> compounds can be enhanced by utilizing polar pharmacological modifiers, i.e., biologically innocent polar moieties that lessen the overall lipophilicity of the (radio) pharmaceutical compounds [5, 7]. In this respect, hydrophilic ligands could exert the same role with minimal disruption of the complexes' structural identity. The phosphine 1,3,5-triaza-7-phosphadamantane (PTA) and its recently synthesized higher homologue 1,4,7-triaza-9-phosphatricyclo[5.3.2.1]tridecane (CAP) [8] are excellent hydrophilic components of transition-metal compounds that are widely used in the fields of organometallic catalysis as well as for pharmaceuticals development [9, 10]. Both PTA and CAP are air-stable, resistant to oxidation, easy to synthesize, and especially PTA is highly water soluble. Upon P-coordination, the remaining three nitrogen atoms can participate in acid-base interactions in aqueous solutions, which can further impact their pharmacokinetic behavior (e.g., biodistribution and cell uptake by cancer cells) [11]. In addition, the nitrogen atoms are reactive under specific conditions, enabling its functionalization (e.g., N-alkylation) and thus, it could be used as a starting point for targeted drug design by tethering biologically active molecules. A further feature that makes CAP particularly interesting is its stereoelectronic properties. CAP combines strong electron-donating ability with an extremely reduced steric hindrance (cone angle = 109°) [12] making this phosphine ligand unique compared to more classical tertiary phosphines.

The coordination chemistry of PTA with transition metals has been extensively reported [9, 13, 14]. In relation to their use as medicinal compounds, ruthenium and platinum have attracted the main focus of relevant research since PTA complexes with these metals exhibit potent anticancer action [15–17]. However, the chemistry of PTA with rhenium is being increasingly investigated thanks to rhenium's promising medical and catalytic applications. PTA complexes have been reported with rhenium in almost all oxidation states ranging from (+VII) to (+I) [18–26]. Concerning *fac*-[Re<sup>I</sup>(CO)<sub>3</sub>]<sup>+</sup> complexes, PTA is coordinated to the metal centre either in combination with other monodentate ligands (e.g., Cl and Br) [27] or as part of the [2 + 1] mixed-ligand approach where three labile aqua ligands on the *fac*-[M(CO)<sub>3</sub>(H<sub>2</sub>O)<sub>3</sub>]<sup>+</sup> synthon are substituted by a bidentate ligand (bid) and PTA [28–32]. Still, the donor atom combinations with PTA in rhenium complexes incorporating the *fac*-[Re(CO)<sub>3</sub>]<sup>+</sup> core remain limited, despite it being the most prominent synthon in radiopharmaceutical and related medicinal chemistry research. As for CAP, its coordination chemistry with rhenium remains largely unexplored and only in combination with monodentate ligands [11].

In addition to the exploration of the [2 + 1] strategy for the design of new Re(I) complexes by using the appropriate ligands, there is an increased interest on the study of intermolecular interactions of Re(I) complexes in the solid state [33–35] based on diverse types of interactions of rhenium complexes with DNA [36, 37]. Similar systematic crystal structure studies [38–40] have revealed the importance of lone pair  $\pi$  and more specifically the role of carbonyl-carbonyl interactions on the supramolecular assembly of Re complexes. In an effort to develop a new platform of hydrophilic model *fac*-[Re(CO)<sub>3</sub>]<sup>+</sup> complexes for radiopharmaceutical and/or medicinal chemistry applications, we report herein a series of novel [2 + 1] rhenium complexes of the general type *fac*-[Re(CO)<sub>3</sub>(bid)P], where P is PTA or CAP used as the polar, hydrophilic modifier and bid is either quinaldic and picolinic acid (representing N, O donor atom set) or diethyldithiocarbamate (representing S, S' donor atom set). To our knowledge, this is also the first time where [2 + 1] mixed-ligand *fac*-[Re(CO)<sub>3</sub>(bid)(X)] complexes are reported with CAP. The syntheses of the corresponding complexes are presented along with their spectroscopic characterization by NMR, IR, and X-ray crystallography. Hirshfeld surface analysis tools were used to elucidate the intermolecular interactions of the synthesized complexes since the type of these interactions can impact the packing of the complexes and their pharmacokinetic behavior.

## 2. Materials and Methods

**2.1. General Information.** All reagents and starting materials were purchased from commercial suppliers and used without further purification. CAP [41], and [NEt<sub>4</sub>]<sub>2</sub>[ReBr<sub>3</sub>CO<sub>3</sub>] [42] were synthesized by following published procedures. All organic solvents were used as supplied (ACS or HPLC grade) unless otherwise noted. IR spectra were recorded on a Nicolet 6700 FT-IR (Thermo Scientific, USA) in the region 4000–500 cm<sup>-1</sup>. <sup>1</sup>H and <sup>13</sup>C-NMR spectra were obtained in DMSO-d<sub>6</sub> at 25°C on a Bruker Avance DRX 500 or 250 MHz spectrometer. All <sup>31</sup>P-NMR spectra were obtained on the 500 MHz spectrometer. The measured chemical shifts are reported in  $\delta$  (ppm), and the residual signal of the solvent was used as the internal calibration standard (DMSO-d<sub>6</sub>: <sup>1</sup>H = 2.50 ppm, <sup>13</sup>C = 39.51 ppm). For the <sup>31</sup>P-NMR, H<sub>3</sub>PO<sub>4</sub> was used as internal reference. All <sup>13</sup>C-NMR spectra were measured with complete proton decoupling. Data of NMR spectra were recorded as follows: *s* = singlet, *d* = doublet, *t* = triplet, *m* = multiplet, *brs* = broad singlet, *br* = broad signal). The coupling constant *J* is reported in hertz (Hz). The designations *quinH* and *picH* denote the protons on the aromatic rings of quinaldic and picolinic acid, respectively. In analogy, the designations *quin* and *pic* demonstrate the carbons on the respective aromatic rings of the (N, O) ligands. Elemental analysis for C, H, and N was conducted on a PerkinElmer 2400 automatic elemental analyzer (PerkinElmer, USA). HPLC analysis was performed on a Waters 600 chromatography system (Waters, USA) coupled to a Waters 2487 Dual  $\lambda$  absorbance detector (Waters, USA). Separations were achieved on a Macherey-Nagel Nucleosil C-18 RP column (250 × 4 mm, 10  $\mu$ m) eluted with a binary

gradient system including water/0.1% TFA (solvent A) and methanol/0.1% TFA as follows: 0-1 minute, 5% B; 1-11 minutes, 5-70% B; 11-26 minutes 70% B; 26-27 minutes 95% B; 27-42 minutes 95% B; 42-45 minutes 95-5% B. Flow rate, 1 ml/minute; UV detection, 254 and 220 nm.

## 2.2. Synthesis of the Rhenium Complexes

**2.2.1. *fac*-[Re(CO)<sub>3</sub>(quin) (H<sub>2</sub>O)], **1**.** Complex **1** was synthesized according to a published procedure [43]. Briefly, [NEt<sub>4</sub>]<sub>2</sub>[ReBr<sub>3</sub>CO<sub>3</sub>] (231 mg, 0.30 mmol) and quinaldic acid (quin) (51.9 mg, 0.30 mmol) were dissolved in H<sub>2</sub>O (15 mL). The reaction mixture was stirred for 1 h at 60°C during which time a yellow precipitate formed. After cooling at room temperature, the yellow precipitate was filtered, washed with cold H<sub>2</sub>O, and dried under vacuum. NMR data are in agreement with those reported in the literature. Yield: 70% (97 mg). RP-HPLC: *t*<sub>R</sub> = 17.0 minutes; IR (cm<sup>-1</sup>): 2027, 1903, 1877, 1644. Anal. Calc. for C<sub>13</sub>H<sub>8</sub>NO<sub>6</sub>Re: C: 33.91%, H: 1.75%, N: 3.04%. Found: C: 33.85%, H: 1.63%, N: 3.15%.

**2.2.2. *fac*-[Re(CO)<sub>3</sub>(quin) (PTA)], **1a**.** Complex **1** (23.0 mg, 0.05 mmol) and PTA (8.0 mg, 0.05 mmol) were dissolved in MeOH (10 mL) and the yellow reaction mixture was refluxed for 2 h. The solvent was removed under reduced pressure to give **1a** after recrystallization from DCM/hexane. Yield: 94% (29 mg). RP-HPLC: *t*<sub>R</sub> = 16.9 minutes. IR (cm<sup>-1</sup>): 2018, 1923, 1874, 1650. Anal. Calc. for C<sub>19</sub>H<sub>18</sub>N<sub>4</sub>O<sub>5</sub>PRE: C: 38.06%, H: 3.03%, N: 9.34%. Found: C: 38.23%, H: 3.15%, N: 9.28%. <sup>1</sup>H-NMR (250 MHz, DMSO-d<sub>6</sub>, ppm): 8.93 (d, *J* = 7.4 Hz, 1H, *quinH*), 8.52 (d, *J* = 7.7 Hz, 1H, *quinH*), 8.41-8.23 (m, 2H, *quinH*), 8.23-8.08 (m, 1H, *quinH*), 8.04-7.83 (m, 1H, *quinH*), 4.29 (brs, 6H, NCH<sub>2</sub>N), 3.76 (brs, 6H, PCH<sub>2</sub>N). <sup>13</sup>C-NMR (63 MHz, DMSO-d<sub>6</sub>, ppm): 194.59 (d, <sup>2</sup>*J*<sub>C-P</sub> = 8.1 Hz, *cis*-carbonyl), 194.44 (d, <sup>2</sup>*J*<sub>C-P</sub> = 8.1 Hz, *cis*-carbonyl), 189.62 (d, <sup>2</sup>*J*<sub>C-P</sub> = 70.1 Hz, *trans*-carbonyl), 172.10 (s, *quinCOO*), 152.1, 146.57, 142.07, 133.05, 130.54, 129.80, 129.66, 127.77, 122.98 (9C *quinCOO*), 71.38 (d, <sup>3</sup>*J*<sub>C-P</sub> = 7.2 Hz, NCH<sub>2</sub>N), 48.52 (d, <sup>1</sup>*J*<sub>P-C</sub> = 14.7 Hz, PCH<sub>2</sub>N). <sup>31</sup>P-NMR (DMSO-d<sub>6</sub>, ppm): -71.65.

**2.2.3. *fac*-[Re(CO)<sub>3</sub>(quin) (CAP)], **1b**.** Complex **1** (46.0 mg, 0.1 mmol) and CAP (21.9 mg, 0.11 mmol) were dissolved in MeOH (10 mL). The orange reaction mixture was refluxed for 2 h and evaporated to dryness under vacuum. Recrystallization from DCM/hexane afforded the product as an orange crystalline solid. Yield: 52% (35.0 mg). RP-HPLC: *t*<sub>R</sub> = 17.5 minutes; IR (cm<sup>-1</sup>): 2019, 1926, 1877, 1646 cm<sup>-1</sup>. Anal. Calc. for C<sub>22</sub>H<sub>24</sub>N<sub>4</sub>O<sub>5</sub>PRE: C: 41.18%, H: 3.77%, N: 8.73%. Found: C: 41.06%, H: 3.69%, N: 8.82%. <sup>1</sup>H-NMR (500 MHz, DMSO-d<sub>6</sub>, ppm): 8.91 (d, *J* = 8.4 Hz, 1H, *quinH*), 8.60 (d, *J* = 8.80 Hz, 1H, *quinH*), 8.32 (d, *J* = 8.4 Hz, 1H, *quinH*), 8.28-8.24 (m, 1H, *quinH*), 8.21-8.16 (m, 1H, *quinH*), 7.98-7.92 (m, 1H, *quinH*), 3.15-2.99 (m, 6H, PCH<sub>2</sub>N), 2.96-2.80 (m, 6H, N(CH<sub>2</sub>)<sub>2</sub>N), 2.71-2.59 (m, 6H, N(CH<sub>2</sub>)<sub>2</sub>N). <sup>13</sup>C-NMR (125.76 MHz, DMSO-d<sub>6</sub>, ppm):

195.76 (d, <sup>2</sup>*J*<sub>C-P</sub> = 5.7 Hz, 2 x *cis*-carbonyls), 190.94 (d, <sup>2</sup>*J*<sub>C-P</sub> = 58.3 Hz, *trans*-carbonyl), 172.06 (*quinCOO*), 152.21, 146.57, 141.84, 133.02, 130.30, 129.70, 129.64, 127.91, 122.79 (9C, *quinCOO*), 50.88 (N(CH<sub>2</sub>CH<sub>2</sub>)N), 50.77 (N(CH<sub>2</sub>CH<sub>2</sub>)N), 48.32 (d, <sup>1</sup>*J*<sub>P-C</sub> = 8.5 Hz, PCH<sub>2</sub>N), <sup>31</sup>P-NMR (DMSO-d<sub>6</sub>, ppm): 38.66.

**2.2.4. *fac*-[Re(CO)<sub>3</sub>(pic) (H<sub>2</sub>O)], **2**.** Complex **2** was synthesized according to a published procedure [44]. Briefly, [NEt<sub>4</sub>]<sub>2</sub>[ReBr<sub>3</sub>CO<sub>3</sub>] (231 mg, 0.30 mmol) and picolinic acid (*pic*) (74 mg, 0.60 mmol) were dissolved in H<sub>2</sub>O (15 mL) and the reaction mixture was stirred for 3 h at 70°C. After cooling to room temperature, the volume of the solvent was reduced to ~3 mL and was placed in the fridge overnight. The yellow precipitate that formed was filtered, washed with cold H<sub>2</sub>O, and dried under vacuum. NMR data are in agreement with that reported in the literature. Yield: 68% (84 mg). RP-HPLC: *t*<sub>R</sub> = 14.9 min; IR (cm<sup>-1</sup>): 2024, 1895, 1874, 164; Anal. Calc. for C<sub>9</sub>H<sub>6</sub>NO<sub>6</sub>Re: C: 26.34%, H: 1.47%, N: 3.41%. Found: C: 26.26%, H: 1.36%, N: 3.38%.

**2.2.5. *fac*-[Re(CO)<sub>3</sub>(pic) (PTA)], **2a**.** Complex **2** (30 mg, 0.07 mmol) and PTA (10 mg, 0.07 mmol) were dissolved in MeOH (7 mL) and the yellowish reaction mixture was refluxed for 2 h. The solvent was then removed under reduced pressure and the residue was recrystallized from DCM/hexane to afford **2a**. Yield: 76% (32.0 mg). RP-HPLC: *t*<sub>R</sub> = 15.2 minutes. IR (cm<sup>-1</sup>): 2022, 1946, 1878, 1650. Anal. Calc. for C<sub>15</sub>H<sub>16</sub>N<sub>4</sub>O<sub>5</sub>PRE: C: 32.79%, H: 2.94%, N: 10.20%. Found: C: 32.65%, H: 3.02%, N: 10.16%. <sup>1</sup>H-NMR (500 MHz, DMSO-d<sub>6</sub>, ppm): 8.81 (brs, 1H, *picH*), 8.34-8.25 (m, 1H, *picH*), 8.11 (d, *J* = 7.2 Hz, 1H, *picH*), 7.89-7.79 (m, 1H, *picH*), 4.42-4.28 (m, 6H, NCH<sub>2</sub>N), 3.84 (brs, 6H, PCH<sub>2</sub>N). <sup>13</sup>C-NMR (125.76 MHz, ppm): 194.78 (d, <sup>2</sup>*J*<sub>C-P</sub> = 7.6 Hz, *cis*-carbonyl), 193.94 (d, <sup>2</sup>*J*<sub>C-P</sub> = 7.6 Hz, *cis*-carbonyl), 190.03 (d, <sup>2</sup>*J*<sub>C-P</sub> = 70.8 Hz, *trans*-carbonyl), 170.87 (*picCOO*), 153.29, 140.80, 129.29, 126.94, 71.49 (d, <sup>3</sup>*J*<sub>P-C</sub> = 6.7 Hz, NCH<sub>2</sub>N), 48.19 (d, <sup>1</sup>*J*<sub>P-C</sub> = 14.4 Hz, PCH<sub>2</sub>N). <sup>31</sup>P-NMR (DMSO-d<sub>6</sub>, ppm): -73.26.

**2.2.6. *fac*-[Re(CO)<sub>3</sub>(pic) (CAP)], **2b**.** Complex **2** (41.0 mg, 0.10 mmol) and CAP (21.9 mg, 0.11 mmol) were dissolved in MeOH (10 mL). The yellow reaction mixture was refluxed for 2 h and the solvent was removed under reduced pressure to give **2b** after recrystallization from DCM/hexane. Yield: 97% (59.0 mg). RP-HPLC: *t*<sub>R</sub> = 15.9 minutes. IR (cm<sup>-1</sup>): 2010, 1891, 1869, 1660. Anal. Calc. for C<sub>18</sub>H<sub>22</sub>N<sub>4</sub>O<sub>5</sub>PRE: C: 36.55%, H: 3.75%, N: 9.47%. Found: C: 36.47%, H: 3.62%, N: 9.53%. <sup>1</sup>H-NMR (500 MHz, DMSO-d<sub>6</sub>, ppm): 8.90 (brs, 1H, *picH*), 8.31-8.21 (m, 1H, *picH*), 8.13-8.05 (m, 1H, *picH*), 7.86-7.77 (m, 1H, *picH*), 3.22-3.11 (m, 6H, PCH<sub>2</sub>N), 3.00-2.89 (m, 6H, N(CH<sub>2</sub>)<sub>2</sub>N), 2.79-2.66 (br, 6H, N(CH<sub>2</sub>)<sub>2</sub>N). <sup>13</sup>C-NMR (125.76 MHz, DMSO-d<sub>6</sub>, ppm): 196.13 (d, <sup>2</sup>*J*<sub>C-P</sub> = 5.1 Hz, *cis*-carbonyl), 195.23 (d, <sup>2</sup>*J*<sub>C-P</sub> = 5.1 Hz, *cis*-carbonyl), 191.38 (d, <sup>2</sup>*J*<sub>C-P</sub> = 59.1 Hz, *trans*-carbonyl), 170.95 (*picCOO*), 153.57, 149.63, 140.62, 129.11, 126.76 (5C, *picCOO*), 51.03 (N(CH<sub>2</sub>CH<sub>2</sub>)N), 50.74

TABLE 1: Crystallographic data for complexes **1b**, **2b**, **3a**, and **3b**.

	<b>1b</b>	<b>2b</b>	<b>3a</b>	<b>3b</b>
Formula	C <sub>22</sub> H <sub>24</sub> N <sub>4</sub> O <sub>5</sub> PRE	C <sub>18</sub> H <sub>22</sub> N <sub>4</sub> O <sub>5</sub> PRE	C <sub>14</sub> H <sub>22</sub> N <sub>4</sub> O <sub>3</sub> PRESe <sub>2</sub>	C <sub>17</sub> H <sub>28</sub> N <sub>4</sub> O <sub>3</sub> PRESe <sub>2</sub>
<i>Fw</i>	641.62	591.56	575.64	617.72
Space group	<i>P</i> 2 <sub>1</sub> / <i>c</i>	<i>P</i> 2 <sub>1</sub>	<i>Pbca</i>	<i>P</i> 2 <sub>1</sub> / <i>c</i>
<i>a</i> (Å)	10.8032 (5)	10.4241 (6)	11.9639 (3)	11.0443 (2)
<i>b</i> (Å)	14.8257 (7)	7.4583 (4)	12.5031 (3)	16.2008 (3)
<i>c</i> (Å)	14.4608 (7)	13.0408 (8)	26.2270 (7)	12.6720 (2)
$\alpha$ (°)	90.0	90.0	90.0	90.0
$\beta$ (°)	98.365 (2)	98.365 (2)	90.0	103.095 (1)
$\gamma$ (°)	90.0	90.0	90.0	90.0
<i>V</i> (Å <sup>3</sup> )	2291.47 (19)	1003.08 (10)	3923.19 (17)	2208.40 (7)
<i>Z</i>	4	2	8	4
<i>T</i> (°C)	20	-113	20	-113
Radiation	Mo K $\alpha$	Mo K $\alpha$	Mo K $\alpha$	Mo K $\alpha$
$\rho_{\text{calcd}}$ (g cm <sup>-3</sup> )	1.860	1.959	1.949	1.858
$\mu$ (mm <sup>-1</sup> )	5.415	6.175	6.510	5.789
$2\theta_{\text{max}}$	54.0°	54.0°	54.0°	54.0°
Reflections collected/unique/used	53018/5011/5011	18362/4349/4349	32531/4253/4253	41273/4812/4812
<i>R</i> <sub>int</sub>	0.0371	0.0252	0.0518	0.0299
Parameters refined	346	278	292	365
Reflections with <i>I</i> > 2 $\sigma$ ( <i>I</i> )	4501	4249	3688	4421
<i>R</i> <sub>1</sub> <sup>a</sup> / <i>wR</i> <sub>2</sub> <sup>a</sup> [ <i>I</i> > 2 $\sigma$ ( <i>I</i> )]	0.0214/0.0461	0.0173/0.0401	0.0231/0.0554	0.0173/0.0358
<i>R</i> <sub>1</sub> <sup>a</sup> / <i>wR</i> <sub>2</sub> <sup>a</sup> (for all data)	0.0252/0.0471	0.0178/0.0403	0.0284/0.0578	0.0201/0.0365
( $\Delta/\sigma$ ) <sub>max</sub>	0.002	0.003	0.001	0.002
( $\Delta\rho$ ) <sub>max</sub> / <sub>min</sub> (e/Å <sup>3</sup> )	0.828/-0.800	0.721/-0.443	0.727/-0.787	0.749/-0.636

<sup>a</sup> $w = 1/[\sigma^2(F_o^2) + (\alpha P)^2 + bP]$  and  $P = [\max(F_o^2, 0) + 2F_c^2]/3$ ,  $a = 0.0192$ ,  $b = 2.3883$  (**1b**);  $a = 0.0134$ ,  $b = 0.5262$  (**2b**);  $a = 0.0281$ ,  $b = 0.7043$  (**3a**);  $a = 0.0143$ ,  $b = 1.7692$  (**3b**);  $R_1 = \sum(|F_o| - |F_c|) / \sum(|F_o|)$  and  $wR_2 = \{\sum[w(F_o^2 - F_c^2)^2] / \sum[w(F_o^2)^2]\}^{0.5}$ .

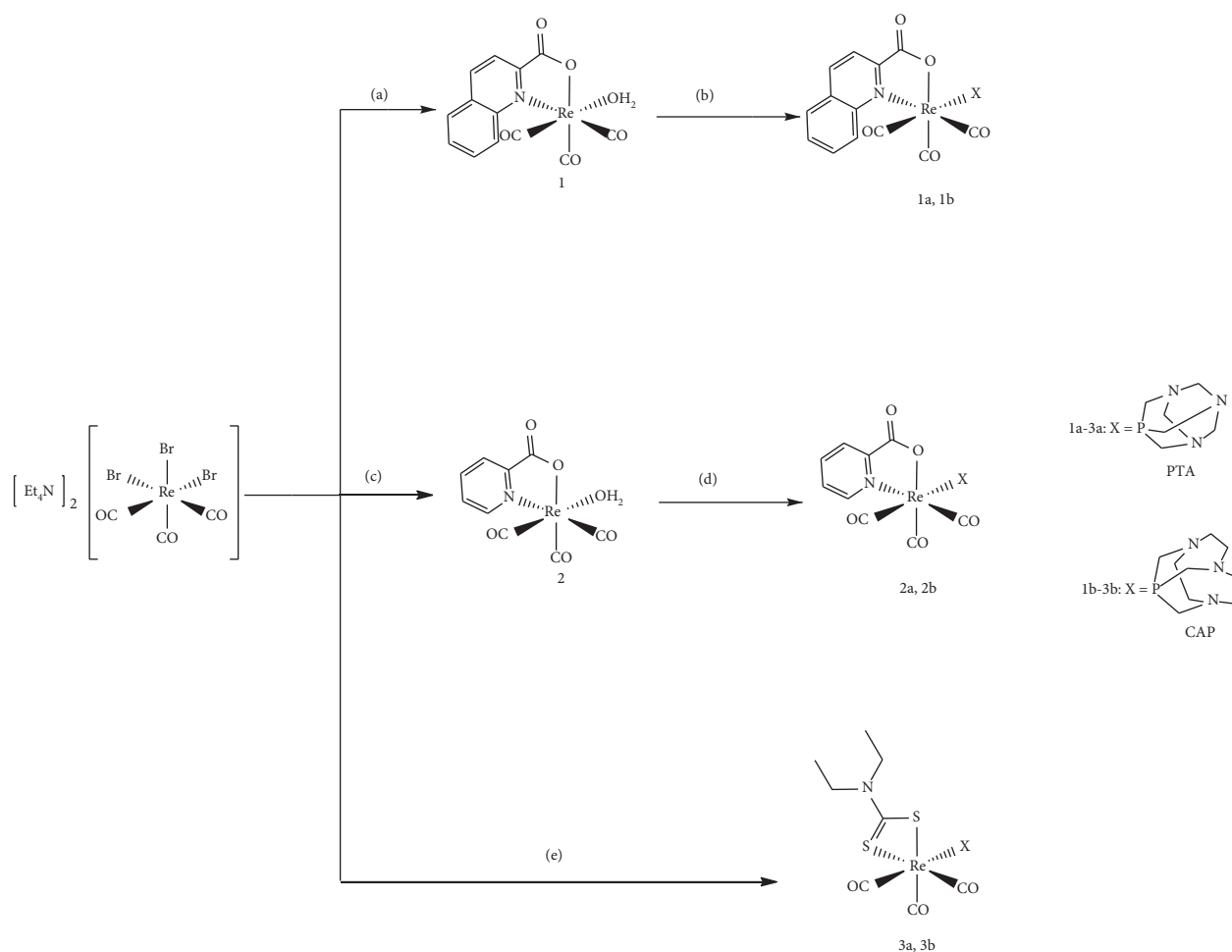
(N(CH<sub>2</sub>CH<sub>2</sub>)N), 47.94 (d, <sup>1</sup>J<sub>C-P</sub> = 8.8 Hz, P(CH<sub>2</sub>)N). <sup>31</sup>P-NMR (DMSO-d<sub>6</sub>, ppm): 37.21.

2.2.7. *fac*-[Re(CO)<sub>3</sub>(Et<sub>2</sub>SS) (PTA)], **3a**. [NEt<sub>4</sub>]<sub>2</sub>[ReBr<sub>3</sub>CO<sub>3</sub>] (77.0 mg, 0.10 mmol), PTA (15.7 mg, 0.10 mmol), and sodium diethyldithiocarbamate trihydrate (Et<sub>2</sub>SS) (22.5 mg, 0.10 mmol) were dissolved in MeOH (4 mL). The reaction mixture was refluxed for 2 h and after cooling to room temperature, the solid that formed was filtered off, washed with cold MeOH, and dried under vacuum. Yield: 42% (25.0 mg). RP-HPLC: *t*<sub>R</sub> = 18.8 minutes. IR (cm<sup>-1</sup>): 2008, 1914, 1878. Anal. Calc. for C<sub>14</sub>H<sub>22</sub>N<sub>4</sub>O<sub>3</sub>PRESe<sub>2</sub>: C: 29.21%, H: 3.85%, N: 9.73%. Found: C: 29.18%, H: 3.72%, N: 9.85%. <sup>1</sup>H-NMR (250 MHz, ppm): 4.46 (s, 6H, NCH<sub>2</sub>N), 4.18 (s, 6H, PCH<sub>2</sub>N), 3.63 (m, 4H, NCH<sub>2</sub>CH<sub>3</sub>), 1.23 (t, <sup>3</sup>J = 7.1 Hz, 6H, NCH<sub>2</sub>CH<sub>3</sub>). <sup>13</sup>C-NMR (63 MHz, DMSO-d<sub>6</sub>, ppm):  $\delta$  = 209.37 (d, <sup>3</sup>J<sub>C-P</sub> = 2 Hz, S=C(S)N), 191.83 (d, <sup>2</sup>J<sub>C-P</sub> = 8.2 Hz, 2 x *cis*-carbonyls), 190.26 (d, <sup>2</sup>J<sub>C-P</sub> = 69.9 Hz, *trans*-carbonyl), 71.91 (d, <sup>3</sup>J<sub>P-C</sub> = 6.5 Hz, NCH<sub>2</sub>N), 49.10 (d, <sup>1</sup>J<sub>P-C</sub> = 16.3 Hz, PCH<sub>2</sub>N), 44.09 (NCH<sub>2</sub>CH<sub>3</sub>), 12.11 (NCH<sub>2</sub>CH<sub>3</sub>). <sup>31</sup>P-NMR (DMSO-d<sub>6</sub>, ppm): -84.56.

2.2.8. *fac*-[Re(CO)<sub>3</sub>(Et<sub>2</sub>SS) (CAP)], **3b**. [NEt<sub>4</sub>]<sub>2</sub>[ReBr<sub>3</sub>CO<sub>3</sub>] (77.0 mg, 0.10 mmol), CAP (21.9 mg, 0.11 mmol) and Et<sub>2</sub>SS (22.5 mg, 0.10 mmol) were dissolved in MeOH (4 mL). The reaction mixture was refluxed for 2 h at which time a yellow precipitate formed. The solid was filtered, washed with cold MeOH, and dried under vacuum. Yield: 45% (29 mg). RP-HPLC: *t*<sub>R</sub> = 19.9 minutes. IR (cm<sup>-1</sup>): 1998, 1898, 1858. Anal.

Calc. for C<sub>17</sub>H<sub>28</sub>N<sub>4</sub>O<sub>3</sub>PRESe<sub>2</sub>: C: 33.05%, H: 4.57%, N: 9.07%. Found: C: 33.16%, H: 4.49%, N: 9.16%. <sup>1</sup>H-NMR (250 MHz, DMSO-d<sub>6</sub>, ppm):  $\delta$  = 3.74–3.47 (m, 10H, NCH<sub>2</sub>CH<sub>3</sub> overlapping with PCH<sub>2</sub>N), 3.14–2.96 (m, 6H, N(CH<sub>2</sub>)<sub>2</sub>N), 2.96–2.75 (m, 6H, N(CH<sub>2</sub>)<sub>2</sub>N), 1.20 (t, <sup>3</sup>J = 7.1 Hz, 6H, NCH<sub>2</sub>CH<sub>3</sub>). <sup>13</sup>C-NMR (63 MHz, DMSO-d<sub>6</sub>, ppm):  $\delta$  = 209.06 (s, SSCN), 193.16 (d, <sup>2</sup>J<sub>C-P</sub> = 6.7 Hz, 2 x *cis*-carbonyls), 191.23 (d, <sup>2</sup>J<sub>C-P</sub> = 57.4 Hz, *trans*-carbonyl), 51.06 (s, N(CH<sub>2</sub>)<sub>2</sub>N), 48.88 (d, <sup>1</sup>J<sub>P-C</sub> = 10.6 Hz, PCH<sub>2</sub>N), 43.94 (s, NCH<sub>2</sub>CH<sub>3</sub>), 12.25 (s, NCH<sub>2</sub>CH<sub>3</sub>). <sup>31</sup>P-NMR (DMSO-d<sub>6</sub>, ppm): 29.17.

2.3. X-ray Crystal Structure Determination. A crystal of **1b** (0.10 × 0.20 × 0.40 mm) and a crystal of **3a** (0.08 × 0.18 × 0.41 mm) were mounted in air. A crystal of **2b** (0.08 × 0.22 × 0.53 mm) and a crystal of **3b** (0.05 × 0.21 × 0.26 mm) were taken from the mother liquor and immediately cooled to -113°C. Diffraction measurements were made on a Rigaku R-AXIS SPIDER Image Plate diffractometer using graphite monochromated Mo K $\alpha$  radiation. Data collection ( $\omega$ -scans) and processing (cell refinement, data reduction, and empirical absorption correction) were performed using the CrystalClear program package [45]. Important crystallographic data are listed in Table 1. The structures were solved by direct methods using SHELXS v.2013/1 and refined by full-matrix least-squares techniques on *F*<sup>2</sup> with SHELXL ver.2014/6 [46, 47]. All hydrogen atoms were located either by difference maps and were refined isotropically or were introduced at the calculated positions



SCHEME 1: Synthesis of complexes **1a-3a** and **1b-3b**. Reactions and conditions: (a) quinH, H<sub>2</sub>O, 60°C, 1 h; (b) X, MeOH, reflux, 2 h; (c) picH, H<sub>2</sub>O, 70°C, 3 h; (d) X, MeOH, reflux, 2 h; (e) Et<sub>2</sub>SS, X MeOH, reflux, 2 h.

as riding on bonded atoms. All non-hydrogen atoms were refined anisotropically. Plots of the structure were drawn using the Diamond 3 program package [48]. The *CrystalExplorer* package V.17.5 [49] was used for the Hirshfeld Surface (HS) analysis studies of **1b**, **2b**, **3a**, and **3b**. For the HS studies, the  $d_{\text{norm}}$  and shape decorated surfaces were used together with the fingerprint plots.  $d_{\text{norm}}$  is a normalized contact distance, defined in terms of  $d_e$ ,  $d_i$  and the Van der Waals (VdW) radii of two atoms at a distance  $d_e$  outside from a point on the surface and at a distance  $d_i$  inside the surface correspondingly [50].

### 3. Results and Discussion

**3.1. Synthesis of the Rhenium Complexes.** The synthesis of the new complexes is depicted in Scheme 1  $[\text{NEt}_4]_2[\text{Re}(\text{CO})_3\text{Br}_3]$  was used as the rhenium starting synthon for all syntheses. Complexes **1a-1b** and **2a-2b** were synthesized via the mono-aqua complexes **1** and **2**, respectively, formed by the reaction of  $[\text{NEt}_4]_2[\text{Re}(\text{CO})_3\text{Br}_3]$  with the corresponding (N, O) ligand in water. The aqua Re complexes were then reacted with equimolar amounts of PTA or CAP in refluxing methanol to afford the final [2 + 1] complexes. However,

complexes **3a-3b** were synthesized more efficiently by a one-pot reaction in methanol, using equimolar amounts of the rhenium precursor, diethyldithiocarbamate, and the corresponding phosphine. Pure compounds were obtained in moderate to excellent yields (42% to 97%) and were characterized by elemental analysis, IR, and NMR-spectroscopy. Crystals suitable for X-ray crystallography were obtained by slow evaporation from DCM/hexane.

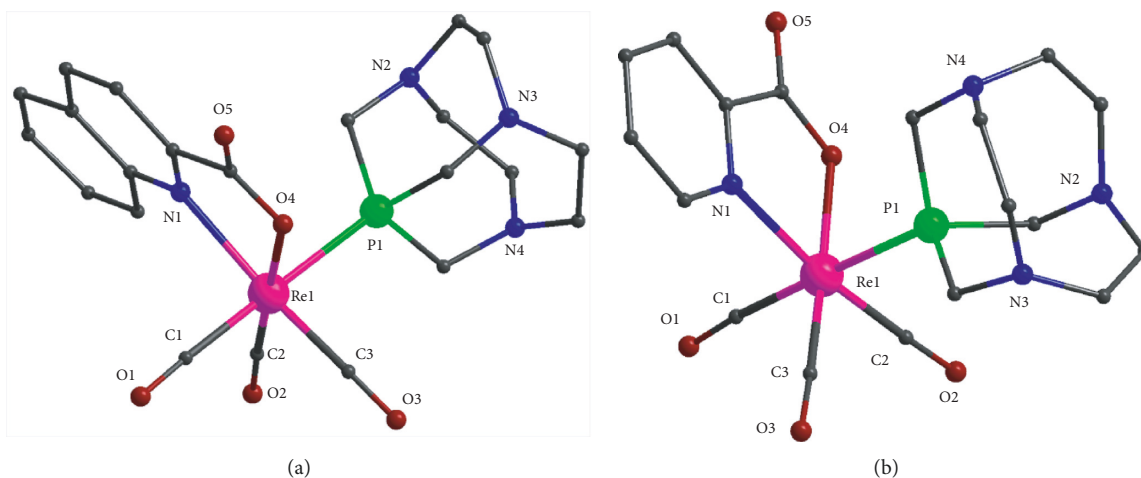
**3.2. IR Characterization.** The IR spectra of all rhenium complexes show the typical pattern for the tricarbonyl *fac*- $[\text{Re}(\text{CO})_3]^+$  moiety with bands in the range of 2013–1870  $\text{cm}^{-1}$  [51, 52]. The presence of the strong band at  $\sim 1604\text{--}1642\text{ cm}^{-1}$  is attributed to the stretching of the carboxylate carbonyl shifted to a lower frequency compared to that of free quinaldic acid at 1695  $\text{cm}^{-1}$  [53] and picolinic acid at 1720  $\text{cm}^{-1}$ .

**3.3. NMR Characterization.** The  $^1\text{H}$ ,  $^{13}\text{C}$ , and  $^{31}\text{P}$ -NMR data obtained for the synthesized complexes are consistent with the proposed structures. Upon coordination of the bidentate and PTA/CAP ligands, characteristic shifts are prominent compared to its non-coordinated states. In the (N, O)

TABLE 2:  $^{31}\text{P}$  and  $^{13}\text{C}$  ( $\text{C} \equiv \text{O}$ ) NMR chemical shifts for PTA, CAP and all Re complexes<sup>a</sup>.

	PTA	CAP	<b>1a</b>	<b>1b</b>	<b>2a</b>	<b>2b</b>	<b>3a</b>	<b>3b</b>
$^{31}\text{P}$	-104.01	47.08	-71.65	38.66	-73.26	37.21	-84.56	29.17
	—	—	194.59 (cis) ( $J = 8.1$ Hz)	195.76 (cis) ( $J = 5.7$ Hz)	194.78 (cis) ( $J = 7.6$ Hz)	196.13 (cis) ( $J = 5.1$ Hz)	191.83 (cis) ( $J = 8.2$ Hz)	193.16 (cis) ( $J = 6.7$ Hz)
$^{13}\text{C}$ ( $\text{C} \equiv \text{O}$ )			194.44 (cis) ( $J = 8.1$ Hz)	190.94 (trans) ( $J = 58.3$ Hz)	193.94 (cis) ( $J = 7.6$ Hz)	195.23 (cis) ( $J = 5.1$ Hz)	190.26 (trans) ( $J = 69.9$ Hz)	191.23 (trans) ( $J = 57.4$ Hz)
			189.62 (trans) ( $J = 70.1$ Hz)		190.03 (trans) ( $J = 70.8$ Hz)	191.38 (trans) ( $J = 59.1$ Hz)		

<sup>a</sup>All spectra are recorded in DMSO-*d*<sub>6</sub>,  $J$  refers to  $^2J_{\text{C-P}}$ , and chemical shifts are in ppm.

FIGURE 1: Partially labelled plots of **1b** (a) and **2b** (b).

complexes, downfield shifts of all aromatic protons of the picolinic and quinaldic acid moiety are noted, attributed to the loss of electron density after coordination of the N-aromatic nitrogen. Coordination of the carboxylate moiety is confirmed by the downfield shift of its carbonyl peak (e.g., 172.10 ppm for complex **1a** compared to the corresponding peak of free quinaldic acid at 167.25 ppm).

The  $^1\text{H}$ -NMR peaks are generally broad indicating a degree of conformational mobility in the compounds and as such, no  $^1\text{H}$ - $^{31}\text{P}$  couplings can be seen for the coordinated phosphine ligands. Nevertheless,  $^{13}\text{C}$ - $^{31}\text{P}$  couplings are present both in the carbonyl peaks and the PTA/CAP carbons of the new complexes. The carbonyl at the *trans*-position to the phosphine ligands couples strongly with the P atom displaying a large coupling constant (e.g.,  $^2J_{\text{C-P}} = 70.1$  Hz at 194.44 ppm for **1a**) while a much smaller one is observed for the carbonyls at *cis*-position (e.g.,  $^2J_{\text{C-P}} = 8.1$  Hz at 194.59 ppm for **1a**) (Table 2), a fact that has been previously reported by us in similar systems [54] and others [55]. Interestingly, this  $^2J_{\text{C-P}}$  coupling is stronger for the PTA complexes compared to the corresponding CAP complexes (e.g.,  $^2J_{\text{C-P}}(\text{trans}) = 58.3$  Hz and  $^2J_{\text{C-P}}(\text{cis}) = 5.7$  Hz for **1b**). In all PTA complexes, the carbons of the phosphine ligand display the expected  $^{13}\text{C}$ - $^{31}\text{P}$  couplings ( $^1J_{\text{C-P}}$  for  $\text{PCH}_2\text{N}$  and  $^3J_{\text{C-P}}$  for  $\text{NCH}_2\text{N}$ ) and appear as doublets. For the CAP complexes,  $^{13}\text{C}$ - $^{31}\text{P}$  couplings are observed only for the  $\text{PCH}_2\text{N}$  carbon, while the  $\text{NCH}_2\text{CH}_2\text{N}$  carbons appear as two differentiated singlets in close proximity (for the N, O

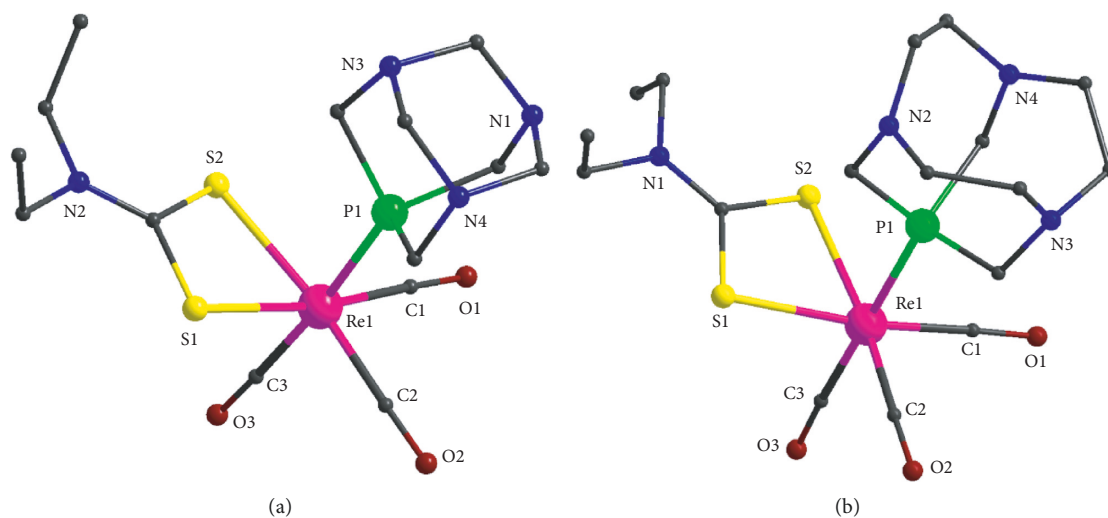
complexes) or as one singlet (for the S, S complex). This difference between the (N, O), and (S, S) complexes with CAP could be attributed to the larger degree of asymmetry due to the bulkier (N, O) ligand.

Finally, the  $^{31}\text{P}$ -NMR data of all PTA complexes (**1a-3a**) display significant downfield shifts compared to the free phosphine ligand due to loss of electron density from the P atom, providing proof of coordination of the phosphorus ligand to the *fac*- $[\text{Re}(\text{CO})_3]^+$  metal centre (Table 2). The large difference between the  $^{31}\text{P}$ -NMR chemical shifts of uncoordinated PTA (-104.01 ppm) and CAP (+47.08 ppm) ligands suggest that these sterically similar phosphanes have substantially different electronic structures [10, 56]. This abnormal behavior is also reflected to the CAP derivatives **1b-3b**. As shown in Table 2, their  $^{31}\text{P}$  resonances are displaced upfield which is unusual among phosphane ligands but is also observed for other CAP complexes [12]. All complexes reported herein show a single  $^{31}\text{P}$  peak demonstrating the absence of isomers, as expected.

**3.4. Description of the Structures.** The molecular structures of **1b** and **2b** are shown in Figure 1; selected bond distances and angles are listed in Table 3. Both complexes consist of the *fac*- $[\text{Re}^1(\text{CO})_3]$  moiety bound to one bidentate (N, O) chelate ligand and to the phosphorus atom of one CAP ligand. The (N, O) chelate ligand in **1b** is the anion of quinaldic acid and in **2b** is the anion of picolinic acid. The coordination

TABLE 3: Selected bond distances (Å) and angles (°) for **1b** and **2b**.

	<b>1b</b>	<b>2b</b>
<i>Distances</i>		
Re (1)-C (2)	1.889 (3)	1.939 (5)
Re (1)-C (3)	1.907 (3)	1.938 (5)
Re (1)-C (1)	1.965 (3)	1.881 (6)
Re (1)-O (4)	2.140 (2)	2.184 (3)
Re (1)-N (1)	2.244 (2)	2.223 (4)
Re (1)-P (1)	2.4543 (8)	2.3910 (12)
<i>Angles</i>		
C (2)-Re (1)-C (3)	83.99 (14)	88.5 (2)
C (2)-Re (1)-C (1)	91.24 (13)	89.6 (2)
C (3)-Re (1)-C (1)	90.66 (14)	90.7 (2)
C (2)-Re (1)-O (4)	179.34 (12)	96.70 (17)
C (3)-Re (1)-O (4)	95.93 (12)	174.01 (18)
C (1)-Re (1)-O (4)	89.42 (11)	92.27 (19)
C (2)-Re (1)-N (1)	105.16 (11)	169.93 (17)
C (3)-Re (1)-N (1)	170.84 (12)	101.50 (19)
C (1)-Re (1)-N (1)	89.65 (11)	91.5 (2)
O (4)-Re (1)-N (1)	74.92 (8)	73.25 (13)
C (2)-Re (1)-P (1)	92.62 (10)	89.88 (16)
C (3)-Re (1)-P (1)	87.63 (11)	88.13 (16)
C (1)-Re (1)-P (1)	175.59 (9)	178.77 (16)
O (4)-Re (1)-P (1)	86.73 (7)	88.90 (10)
N (1)-Re (1)-P (1)	91.40 (6)	89.24 (10)

FIGURE 2: Partially labelled plots of **3a** (a) and **3b** (b).

geometry around the  $\text{Re}^{\text{I}}$  ion is distorted octahedral in both **1b** and **2b**. There are two short Re-CO bond distances ( $\sim 1.90$  Å) in **1b** which are in the *trans*-position with respect to the (N, O) donor atoms of quinaldato ligand and one longer Re-CO distance at  $\sim 1.94$  Å which is in the *trans*-position to the Re-P bond. The Re-(N, O) bond distances are  $\sim 2.24$  and  $\sim 2.14$  Å, respectively. The Re-P bond distance is the longest in the coordination sphere ( $\sim 2.45$  Å). The *cis*-angles in the coordination sphere are in the range  $\sim 75$ – $105^\circ$  and the *trans*-angles are  $170.84(12)$ ,  $175.59(9)$ , and  $179.34(12)^\circ$ . The five-membered ring in the coordination sphere, defined by Re-N-C-C-O, is almost planar with the largest deviation  $\sim 0.11$  Å for C(4). In **2b**, there are two long

Re-CO bond distances ( $\sim 1.94$  Å), *trans* to the (N, O) donor atoms of picolinato ligand, and one shorter Re-CO distance at  $\sim 1.88$  Å which is *trans* to the Re-P bond. The Re-(N, O) bond distances are  $\sim 2.22$  and  $\sim 2.18$  Å, respectively, and the Re-P bond distance is the longest in the coordination sphere ( $\sim 2.39$  Å). The *cis*-angles in the coordination sphere are in the range  $\sim 73$ – $101^\circ$  and the *trans*-angles are  $169.93(17)$ ,  $174.01(18)$ , and  $178.77(16)^\circ$ . The five-membered ring in the coordination sphere, defined by Re-N-C-C-O, is almost planar with the largest deviation  $\sim 0.05$  Å for C(4).

The molecular structures of **3a** and **3b** are shown in Figure 2; selected bond distances and angles are listed in Table 4. Both complexes consist of the *fac*- $[\text{Re}^{\text{I}}(\text{CO})_3]$  moiety

TABLE 4: Selected bond distances (Å) and angles (°) for **3a** and **3b**.

	<b>3a</b>	<b>3b</b>
<i>Distances</i>		
Re (1)-C (1)	1.911 (3)	1.923 (3)
Re (1)-C (2)	1.920 (3)	1.905 (3)
Re (1)-C (3)	1.952 (3)	1.955 (3)
Re (1)-P (1)	2.4375 (7)	2.4584 (6)
Re (1)-S (2)	2.5069 (8)	2.5245 (6)
Re (1)-S (1)	2.5232 (8)	2.5236 (6)
<i>Angles</i>		
C (1)-Re (1)-C (2)	87.90 (14)	89.43 (11)
C (1)-Re (1)-C (3)	90.63 (14)	91.10 (11)
C (2)-Re (1)-C (3)	92.42 (13)	89.04 (11)
C (1)-Re (1)-P (1)	92.11 (10)	88.73 (8)
C (2)-Re (1)-P (1)	91.48 (9)	91.91 (8)
C (3)-Re (1)-P (1)	175.32 (10)	179.02 (8)
C (1)-Re (1)-S (2)	101.80 (10)	101.26 (7)
C (2)-Re (1)-S (2)	170.30 (10)	168.15 (8)
C (3)-Re (1)-S (2)	87.48 (10)	95.77 (8)
P (1)-Re (1)-S (2)	88.25 (2)	83.32 (2)
C (1)-Re (1)-S (1)	171.10 (10)	171.03 (7)
C (2)-Re (1)-S (1)	100.42 (10)	99.50 (8)
C (3)-Re (1)-S (1)	92.16 (10)	89.90 (8)
P (1)-Re (1)-S (1)	84.58 (3)	90.12 (2)
S (2)-Re (1)-S (1)	69.89 (3)	69.764 (19)

TABLE 5: Hydrogen-bond geometry (Å, °) for **1b**, **2b**, **3a**, and **3b**.

D—H...A	D—H (Å)	H...A (Å)	D...A (Å)	D—H...A (°)	Symmetry operation
<b>Complex-1b</b>					
C <sub>18</sub> —H <sub>18A</sub> ...O <sub>2</sub> <sup>i</sup>	0.97	2.49	3.421 (5)	161	(i): $x, -y + 0.5, z + 0.5$
C <sub>14</sub> —H <sub>14B</sub> ...O <sub>2</sub> <sup>ii</sup>	0.96 (5)	2.59 (5)	3.470 (5)	151 (4)	(ii): $x, -y + 1/2, z + 1/2$
C <sub>9</sub> —H <sub>9</sub> ...O <sub>5</sub> <sup>iii</sup>	0.85 (3)	2.48 (3)	3.308 (5)	162 (3)	(iii): $-x, 0.5 + y, 1.5 - z$
C <sub>19</sub> —H <sub>19</sub> ...Cg <sub>1</sub> <sup>iv</sup> (Cg <sub>1</sub> : centroid of C <sub>8</sub> C <sub>13</sub> phenyl ring)	0.97 (1)	3.009 (1)	3.887 (5)	151.3 (3)	(iv): $1 - x, -0.5 + y, 1.5 - z$
<b>Complex-2b</b>					
C <sub>12</sub> —H <sub>12B</sub> ...O <sub>2</sub> <sup>i</sup>	0.99	2.55	3.434 (9)	149	(i): $-x + 1, y - 1/2$
C <sub>14</sub> —H <sub>14A</sub> ...O <sub>5</sub> <sup>ii</sup>	0.99	2.56	3.521 (9)	164	(ii): $-x + 1, y - 1/2, -z + 1$
C <sub>15</sub> —H <sub>15B</sub> ...O <sub>5</sub> <sup>iii</sup>	0.99	2.46	3.411 (9)	162	(iii): $-x + 1, y - 1/2, -z + 1$
C <sub>6</sub> —H <sub>6</sub> ...O <sub>5</sub> <sup>iv</sup>	0.97 (5)	2.56 (5)	3.210 (7)	125 (4)	(iv): $2 - x, -0.5 + y, 1 - z$
C <sub>8</sub> —H <sub>8</sub> ...O <sub>4</sub> <sup>v</sup>	0.77 (6)	2.62 (6)	3.079 (7)	120 (5)	(v): $x, -1 + y, z$
C <sub>9</sub> —H <sub>9</sub> ...O <sub>1</sub> <sup>vi</sup>	1.05 (8)	2.50 (7)	3.104 (7)	116 (5)	(vi): $2 - x, -0.5 + y, 2 - z$
C <sub>8</sub> —H <sub>8</sub> ...C <sub>1</sub> <sup>vii</sup>	0.77 (6)	2.92 (6)	3.682 (9)	170 (5)	(vii): $x, -1 + y, z$
C <sub>13</sub> —H <sub>13</sub> ...Cg <sub>2</sub> <sup>viii</sup>	0.99 (1)	3.4366 (2)	4.154 (9)	130.0 (4)	(viii): $1 - x, 0.5 + y, 1 - z$
C <sub>16</sub> —H <sub>16</sub> ...Cg <sub>2</sub> <sup>ix</sup> (Cg <sub>2</sub> : Centroid of N <sub>1</sub> , C <sub>5</sub> ...C <sub>9</sub> pyridine ring)	0.99 (1)	3.2873 (2)	4.211 (1)	156.0 (6)	(ix): $-1 + x, y, z$
<b>Complex-3a</b>					
C <sub>9</sub> —H <sub>9A</sub> ...N <sub>4</sub> <sup>i</sup>	0.97 (4)	2.68 (4)	3.627 (4)	166 (2)	(i) $-x + 1/2, y - 1/2, z$
C <sub>9</sub> —H <sub>9B</sub> ...N <sub>3</sub> <sup>ii</sup>	0.94 (4)	2.53 (4)	3.413 (4)	158 (3)	(ii) $x - 1/2, y, -z + 1/2$
C <sub>13</sub> —H <sub>13A</sub> ...O <sub>1</sub> <sup>iii</sup>	1.00 (3)	2.56 (3)	3.534 (5)	165 (3)	(iii) $-x + 1/2, y + 1/2$
<b>Complex-3b</b>					
C <sub>5</sub> —H <sub>5A</sub> ...S <sub>2</sub> <sup>i</sup>	1.02 (3)	2.80 (3)	3.701 (3)	147 (2)	(i): $x, -y + 1/2, z - 1/2$
C <sub>8</sub> —H <sub>8A</sub> ...O <sub>2</sub> <sup>iii</sup>	0.97 (4)	2.48 (4)	3.434 (4)	168 (3)	(ii) $-x + 1, -y + 1, -z + 1$
C <sub>6</sub> —H <sub>6B</sub> ...N <sub>2</sub> <sup>ii</sup>	0.95 (4)	2.67 (4)	3.580 (4)	160 (3)	(iii) $x + 1, -y + 1/2, z + 1/2$

which is bound to the (S, S) chelate bidentate ligand (diethyldithiocarbamate) and the phosphorus atom of one PTA or CAP ligand (**3a** or **3b**). The coordination geometry around the Re<sup>I</sup> ion is distorted octahedral in both complexes. There are two short Re-CO bonds in both **3a** and **3b** with bond

distances ~1.91–1.92 Å which are in the *trans*-position with the two sulfur atoms of the diethyldithiocarbamate ligand. The longer Re-CO bond with length ~2.44–2.46 Å is in the *trans*-position to the phosphorous atom of PTA or CAP. The two Re-S bonds are the longest in the coordination sphere



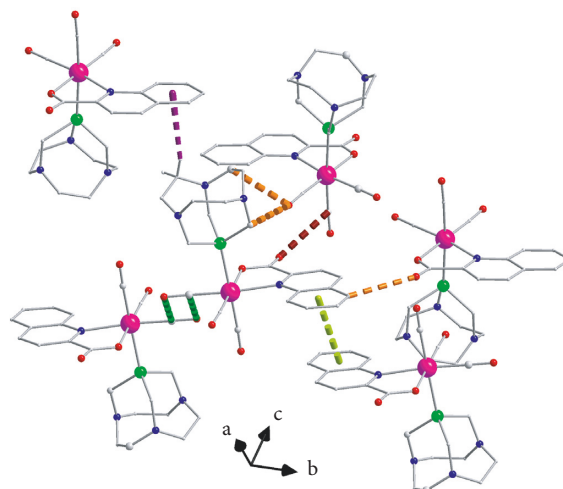


FIGURE 3: Intermolecular interactions observed in the structure of compound **1b**. Dashed thick dark green (antiparallel  $C_3-O_3 \cdots C_3-O_3$ ) and dark red lines indicate carbonyl-carbonyl interactions ( $C-O_5 \cdots C_1-O_1$ ). Dark violet dashed lines indicate  $C_{19}-H_{19} \cdots \pi$  interactions. Light green dashed lines indicate  $\pi \cdots \pi$  between quinaldic ligands and orange dashed lines indicate  $C_{18}-H_{18}A \cdots O_2$ ,  $C_{14}-H_{14}B \cdots O_2$  and  $C_9-H_9 \cdots O_5$  hydrogen bonds.

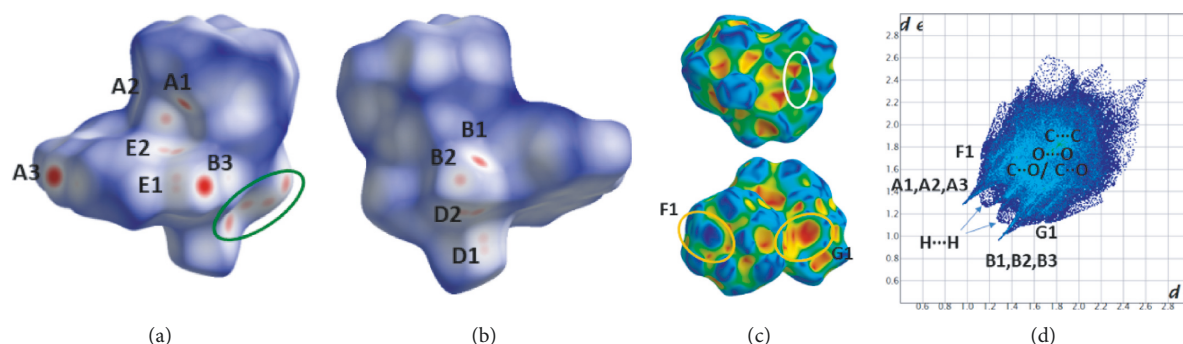


FIGURE 4: (a), (b) Different views of the dnorm decorated HS, (c) two views of the shape decorated HS, and (d) fingerprint plot for the **1b** complex. A1, A2, A3 and B1, B2, B3 are the donor and acceptor contact points of  $C_{18}-H_{18}(A) \cdots O_2$ ,  $C_{14}-H_{14}(B) \cdots O_2$ ,  $C_9-H_9 \cdots O_5$  hydrogen bond interactions. The green ellipse in (a) indicates the area of antiparallel  $CO \cdots CO$ ,  $C_3 \equiv O_3$  carbonyl interactions. E1, E2 and D1, D2 are the donor and acceptor contact points involved in the  $M-C \cdots CO$ ,  $O_5 \cdots C_1^{III}$  type of interactions. The white and orange ellipses in (c) indicate  $\pi \cdots \pi$  and  $C-H \cdots \pi$  (F1 and G1 are donor and acceptor contact points, respectively, Table 5) type of interactions.

$\sim 2.52$  Å in both complexes. The *cis*-angles in the coordination sphere are in the range  $\sim 69$ – $102^\circ$  and the *trans*-angles are in the range  $170$ – $179^\circ$ . The four-membered ring in the coordination sphere, defined by Re-S-C-S atoms, is essentially planar in both complexes with the carbon atom lying  $\sim 0.02$  and  $\sim 0.05$  Å out of the best mean plane of the four atoms.

Comparing the Re-P bond length between the complexes synthesized, the following trends can be noted: (i) the Re-P bond length between PTA and CAP complexes that carry the same bidentate ligand (**3a** and **3b**) does not differ significantly, i.e., 2.4375 for **3a** and 2.4584 for **3b**; (ii) the Re-P bond length of the PTA complex **3a** is similar to other *fac*-[Re(CO)<sub>3</sub>(bid)PTA] complexes reported in the literature [6, 30]; and (iii) the Re-P bond length of all PTA and CAP complexes synthesized herein is consistently shorter compared to other *fac*-[Re(CO)<sub>3</sub>(bid)P] reported in the literature where P is a phosphine other than PTA and CAP, e.g., PPh<sub>3</sub>, P(Cy)<sub>3</sub>, P(Cy)<sub>2</sub>Ph [6, 30, 43] which is possibly attributed to the better  $\sigma$ -donating properties of PTA and CAP.

The intermolecular interactions in the structures of **1b**, **2b**, **3a**, and **3b** present interesting characteristics and their geometrical characteristics are listed in Table 5 for all structures. These interactions are also studied by using HS analysis tools. Figure 3(a) presents the intermolecular interactions observed in the structure of compound **1b** among the complexes. In addition to commonly observed hydrogen bond,  $C-H \cdots \pi$  (Figure 3, Table 5), and  $\pi \cdots \pi$  interactions [the distance between neighboring centrosymmetrically related quinaldic ligands is 3.467(8) Å, symmetry code (v):  $-x, 1-y, 1-z$ , Figure 3], the  $lp(O)-\pi$  type interactions between carbonyls coordinated to transition metals [39, 57] are also observed. The  $C_3 \equiv O_3$  carbonyls are involved in antiparallel  $CO \cdots CO$  interactions [57],  $C_3 \cdots O_3^{vi}$  distance [ $=C_3^{vi} \cdots O_3$ , symmetry code (vi):  $-x, -y, 1-z$ ] equals to 3.104(5) Å, which is less than the sum ( $=3.22$  Å) of van der Waals (vdW) of C ( $=1.7$  Å) and O ( $=1.52$ ) atoms] and  $M-C \cdots CO$  type with the distance  $O_5 \cdots C_1^i$  and the angle  $O_5-C_1^i-O_1^i$  (symmetry code(i):  $x, 0.5-y, 0.5+z$ ) equal to 3.157(4)

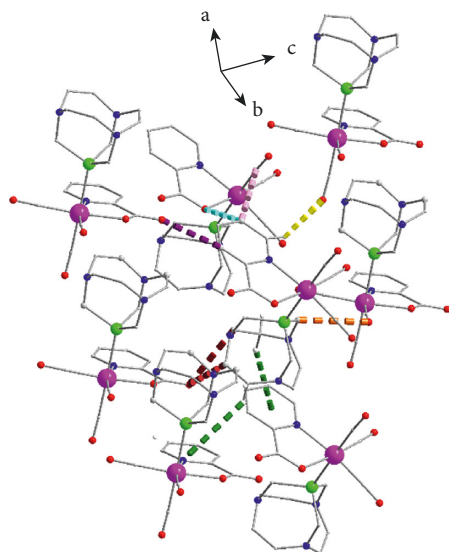


FIGURE 5: Intermolecular interactions among neighboring clusters in the structure of compound **2b**. The different type of hydrogen bond interactions is indicated with dashed thick orange ( $C_{12}-H_{12}\cdots O_2$ ), dark red ( $C_{14}-H_{14}A\cdots O_5$  and  $C_{15}-H_{15}B\cdots O_5$  pairs of interactions), and cyan ( $C_8-H_8\cdots O_4$ ) dashed lines. The pink dashed lines indicate carbonyl  $C_8-H_8\cdots C_1$  type of interactions.  $C_6-H_6\cdots O_5$ ,  $C_9-H_9\cdots O_1$  and  $C_{16}-H_{16}\cdots Cg_2$  ( $C-H\cdots\pi$  type of interactions) are indicated with violet, yellow, and dark green dashed lines, respectively.

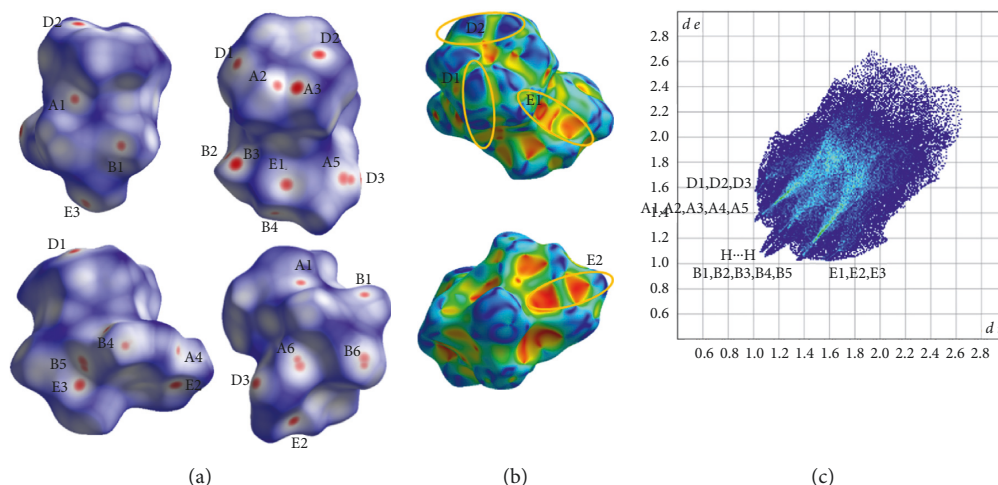


FIGURE 6: (a) Different views of the  $d_{norm}$  decorated HS, (b) two views of the shape decorated HS and (c) fingerprint plot for the **2b** complex. A1, A2, A3, A4, A5, A6 and B1, B2, B3, B4, B5, B6 are the donor and acceptor contact points of  $C_{12}-H_{12}B\cdots O_2$ ,  $C_{14}-H_{14}A\cdots O_5$ ,  $C_{15}-H_{15}B\cdots O_5$ ,  $C_6-H_6\cdots O_5$ ,  $C_8-H_8\cdots O_4$  and  $C_9-H_9\cdots O_1$  hydrogen bond interactions. E1, E2 and D1, D2 are the donor and acceptor contact points involved in the  $C_{13}-H_{13}\cdots Cg_2$  and  $C_{16}-H_{16}\cdots Cg_2$   $C-H\cdots\pi$  type of interactions. E3 and D3 are the donor and acceptor contact points of  $C_8-H_8\cdots C_1$  type of interactions.

Å and  $70.8(2)^\circ$  which are close to the usual one [39]. Through these intermolecular interactions, a layer of complexes is formed parallel to the (100) crystallographic plane (Figure S1a). These layers are stacked parallel to [100] crystallographic direction interacting through  $C-H\cdots\pi$  interactions (Table 5, Figure S1b). The fingerprint plot calculated from HS of complex **1b** is presented in Figure 4(d) where the contribution of each type of intermolecular interactions is indicated. The percentage contribution of the different type of interactions  $H\cdots H$ ,  $O\cdots H/H\cdots O$ ,  $C\cdots H/H\cdots C$ ,  $C\cdots O/O\cdots C$ ,  $O\cdots O$ ,  $C\cdots C$ ,  $N\cdots H/H\cdots N$  are 42.4, 30.3, 12.5, 5.2, 3.7, 2.9, and 2.9%, respectively. All types of interactions

discussed above are also clearly seen on the  $d_{norm}$  HS representation (Figures 4(a) and 4(b)). On the Shape decorated HS, the characteristic blue and red triangles of  $\pi\cdots\pi$  interactions and the complementary red (concave) and blue (convex) areas characteristic of  $C-H\cdots\pi$  interactions are present (Figure 4(c)).

In the structure of compound **2b**, an extensive network of intermolecular interactions is observed such as hydrogen bond and  $C-H\cdots\pi$  type (Table 5, Figure 5). Layers of complexes are formed parallel to the (100) plane through the hydrogen bond  $C_{12}-H_{12}B\cdots O_2$ ,  $C_{14}-H_{14}A\cdots O_5$ ,  $C_{15}-H_{15}B\cdots O_5$ ,  $C_8-H_8\cdots O_4$  and  $C-H\cdots\pi$  type of interactions,

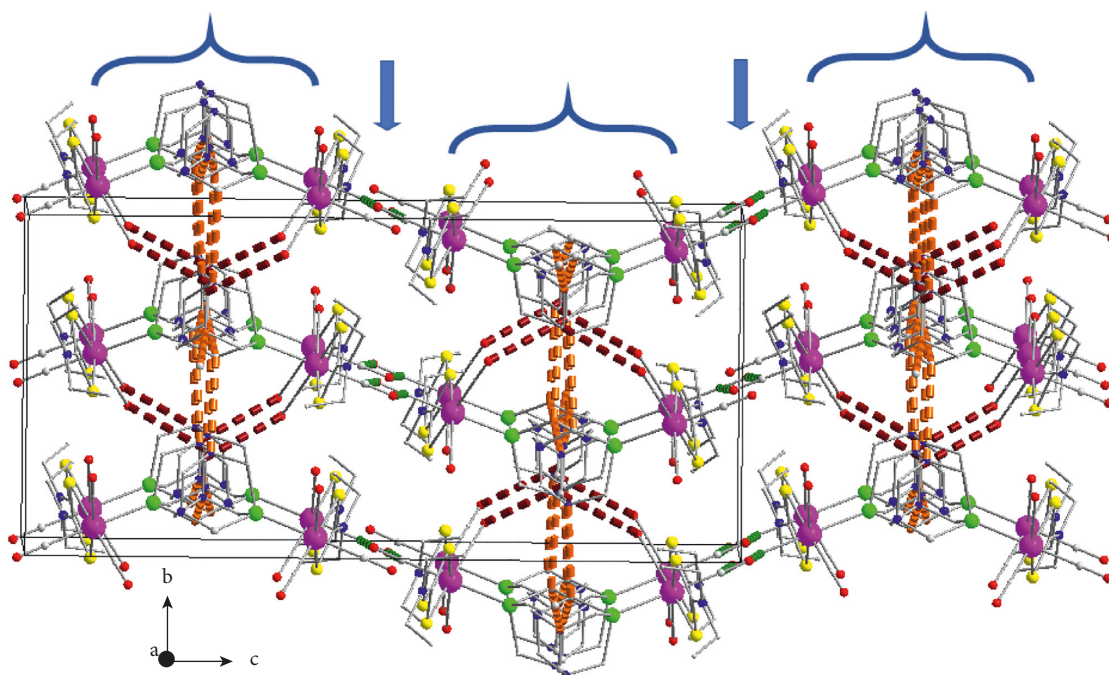


FIGURE 7: Stacking of layers along the *c* crystallographic axis in the structure of compound **3a**. Braces indicate the position of layers and arrows the carbonyl-carbonyl interactions. The dashed thick orange lines indicate  $C_9-H_9A \cdots N_4$  and  $C_9-H_9B \cdots N_3$  and the dark red one indicates  $C_{13}-H_{13}A \cdots O_1$  hydrogen bonds. Dashed thick dark green lines indicate antiparallel  $CO \cdots CO$  carbonyl-carbonyl interactions. Details for the arrangement of complexes and the intermolecular interactions within the layer are presented in Figure S3.

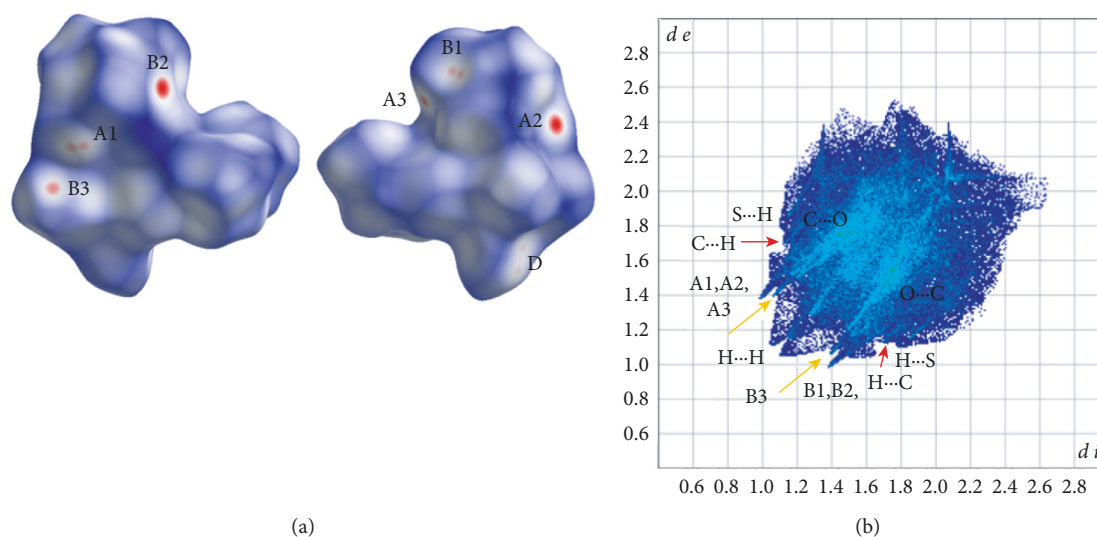


FIGURE 8: (a), Different views of the  $d_{norm}$  decorated HS and (b) fingerprint plot for the **3a** complex. A1, A2, A3 and B1, B2, B3 are the donor and acceptor contact points of  $C_9-H_9(A) \cdots N_4$ ,  $C_9-H_9(B) \cdots N_3$  and  $C_{13}-H_{13}A \cdots O_1$  (indicated with orange arrows in fingerprint plot) hydrogen bond interactions (Table 5). Label D indicates the area of antiparallel  $CO \cdots CO$ ,  $C_3 \equiv O_3$  carbonyl interactions. Red arrows in the fingerprint plot indicate the  $C \cdots H / \cdots C$  contact points.

i.e.,  $C_{13}-H_{13} \cdots Cg_2$ ,  $C_{16}-H_{16} \cdots Cg_2$  (Figure S2a, Table 5). C-H carbonyl type of interactions is also contributing in the formation of these layers ( $C_8-H_8 \cdots C1$ , Figure 5, S2a, Table 5). Neighboring layers are stacked along the *a* crystallographic axis interacting through hydrogen bond  $C_6-H_6 \cdots O_5$ ,  $C_9-H_9 \cdots O_1$  and C-H  $C-H \cdots \pi$  type of interactions, i.e.,  $C_{16}-H_{16} \cdots Cg_2$  (Figure S2b, Table 5). The percentage

contribution of  $H \cdots H$ ,  $O \cdots H / H \cdots O$ ,  $C \cdots H / H \cdots C$ ,  $N \cdots H / H \cdots N$ ,  $O \cdots O$ ,  $C \cdots O / O \cdots C$  contacts, based on the fingerprint plot analysis (Figure 6(c)) are 32.9, 45.6, 14.0, 2.6, 2.2, and 1.9%, respectively and the contact points of the most characteristic interactions are indicated in  $d_{norm}$  decorated HS in Figure 6(a). C-H  $\cdots \pi$  interactions reveal their presence in the characteristic complementary red (concave) and blue

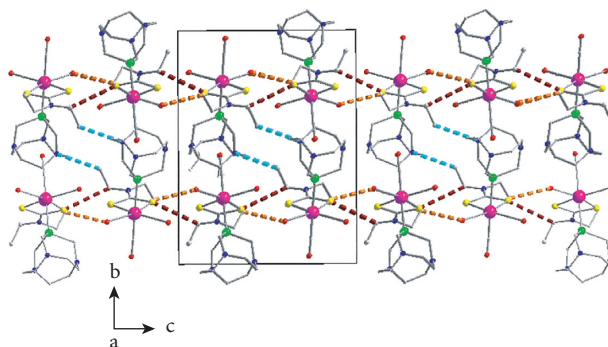


FIGURE 9: Stacking of layers along the *b* crystallographic axis in the structure of compound **3b**, The dashed thick orange, dark red, and cyan lines indicate  $C_8-H_8A \cdots O_2$ ,  $C_5-H_5 \cdots S_2$  and  $C_6-H_6B \cdots N_2$  hydrogen bonds, respectively. Details for the arrangement of complexes and the intermolecular interactions within the layer are presented in Figure S4.

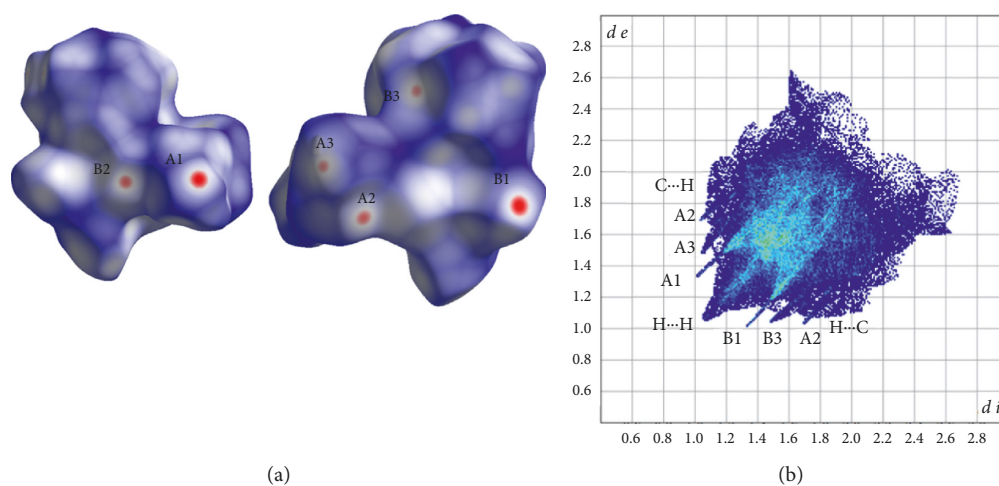


FIGURE 10: (a) Different views of the  $d_{norm}$  decorated HS and (b) fingerprint plot for the **3b** complex. A1, A2, A3 and B1, B2, B3 are the donor and acceptor contact points of  $C_8-H_8A \cdots O_2$ ,  $C_5-H_5A \cdots S_2$  and  $C_6-H_6B \cdots N_2$  hydrogen bond interactions (Table 5).

(convex) areas on the HS decorated with Shape property (Figure 6(b)).

In the structure of **3a**, layers of complexes are formed parallel to the (001) plane through hydrogen bond interactions (Figure S3, Table 5). These layers are stacked along the *c* crystallographic axis (Figure 7) and complexes belonging to neighboring layers interact through antiparallel  $CO \cdots CO$  interactions, where the  $C_3 \equiv O_3$  carbonyls are involved ( $C_3 \cdots O_3^*$  distance is equal to 3.180(4)Å). The percentage contribution of  $H \cdots H$ ,  $O \cdots H/H \cdots O$ ,  $S \cdots H/H \cdots S$ ,  $N \cdots H/H \cdots N$ ,  $C \cdots H/H \cdots C$ ,  $C \cdots O/O \cdots C$ ,  $C \cdots S/S \cdots C$ ,  $O \cdots S/S \cdots O$  contacts derived from fingerprint plot analysis (Figure 8(b)) are 38.0, 31.5, 8.6, 7.8, 7.1, 2.3, 1.4, and 1.0%, respectively. The most intense interactions, i.e.,  $C_9-H_9A \cdots N_4$ ,  $C_9-H_9AB \cdots N_3$  and  $C_{13}-H_{13A} \cdots O_1$  appear on the  $d_{norm}$  decorated HS in Figure 8(a).

In the case of **3b**, complexes interacting through the  $C_8-H_8A \cdots O_2$  and  $C_5-H_5A \cdots S_2$  hydrogen bonds (Table 5) form layers parallel to the plane (010) (Figure S4) and through the  $C_6-H_6B \cdots N_2$  interactions of complexes belonging to neighboring layers stacked along the *b* axis, the 3D architecture of the structure is built (Figure 9). The percentage contribution of  $H \cdots H$ ,  $O \cdots H/H \cdots O$ ,  $C \cdots H/H \cdots C$ ,  $S \cdots H/$

$H \cdots S$ ,  $N \cdots H/H \cdots N$  contacts derived from fingerprint plot analysis (Figure 10(b)) are 49.2, 29.7, 7.7, 7.0, and 2.5, respectively. Each one of  $C \cdots O/O \cdots C$ ,  $C \cdots S/S \cdots C$ ,  $O \cdots S/S \cdots O$  type of contacts contributes less than 1%. The most intense interactions, i.e.,  $C_8-H_8A \cdots O_2$ ,  $C_5-H_5A \cdots S_2$  and  $C_6-H_6B \cdots N_2$  appear on the  $d_{norm}$  decorated HS in Figure 10(a), and as spikes in the fingerprint plot (Figure 10(b)).

#### 4. Conclusions

In this work, the coordination chemistry of rhenium with the hydrophilic monodentate phosphines PTA and CAP was explored by synthesizing and characterizing a series of novel [2 + 1] mixed-ligand *fac*-[ $Re(CO)_3(bid)(X)$ ] complexes. Both PTA and CAP serve the role of the polar and hydrophilic modifier aiming to develop a new platform of hydrophilic *fac*-[ $Re(CO)_3$ ] complexes with favorable pharmacokinetics. The detailed crystal structure studies using the Hirshfeld surface analysis tools have revealed that the  $C-H \cdots O$  type of intermolecular interactions has the largest contribution in the packing of complexes. In the case of **1b**,  $\pi \cdots \pi$  are one type of the characteristic intermolecular interactions that contribute to the packing of complexes and

for the rest are the C-H... $\pi$ . In all structures, the PTA and CAP ligands are coordinated through the P atom with Re and the observation of N...H type of interactions in all studied structures reveals the potential of these three nitrogen atoms to develop hydrogen bonds with their environment and thus to impact the pharmacokinetic behavior of these compounds. In the case of **1b** and **3b**, carbonyl-carbonyl intermolecular interactions are observed among the complexes, which is a type of interaction which recently is discussed as a potential path which could impact the biological and physical properties of these compounds.

This system could potentially be applied in (radio) pharmaceutical design to develop complexes with suitable properties for diagnosis ( $^{99m}\text{Tc}$ ), radiotherapy ( $^{186/188}\text{Re}$ ), and chemotherapy ( $^{185/187}\text{Re}$ ) by tethering a biologically active molecule either to the bidentate or the phosphine ligand. The transfer of the coordination chemistry at the  $^{99m}\text{Tc}$  level, the evaluation of the hydrophilicity of the corresponding complexes, and the investigation of its *in vivo* performance are currently in progress.

### Data Availability

Crystallographic data for the structures reported in this manuscript have been deposited with the Cambridge Crystallographic Data Centre under the CCDC numbers: 2152941 (compound **1b**), 2152938 (compound **2b**), 2152939 (compound **3a**), and 2152940 (compound **3b**). Copies of these data can be obtained free of charge from [https://www.ccdc.cam.ac.uk/data\\_request/cif](https://www.ccdc.cam.ac.uk/data_request/cif).

### Conflicts of Interest

The authors declare that they have no conflicts of interest.

### Acknowledgments

This research was cofinanced by Greece and the European Union (European Social Fund-ESF) through the Operational Programme «Human Resources Development, Education and Lifelong Learning 2014–2020» in the context of the project “Targeting the kynurenine pathway for tumor imaging and characterization by single photon emission computed tomography (SPECT) and positron emission tomography (PET)” (MIS 5047830). The authors thank Dr. Maria Pelecanou for helpful discussions and advice regarding NMR characterization.

### Supplementary Materials

Figure S1: Intermolecular interactions in the structure of compound **1b** forming (a) layers of complexes parallel to the crystallographic plane (100) and (b) Stacks of layers along the a crystallographic axis. Figure S2: (a) Intermolecular interactions among neighboring clusters forming layers of complexes arranged parallel to the crystallographic plane (100), and (b) stacking of layers along the a crystallographic axis in the structure of compound **2b** through hydrogen bond, C-H... $\pi$  type, and carbonyl interactions. Figure S3: Layers of complexes arranged parallel to the crystallographic

plane (001) in the structure of compound **3a** through hydrogen bond interactions. Figure S4: Layers of complexes arranged parallel to the crystallographic plane (010) in the structure of compound **3b**. (*Supplementary Materials*)

### References

- [1] N. Lepareur, F. Laccœuille, C. Bouvry et al., “Rhenium-188 labeled radiopharmaceuticals: current clinical applications in oncology and promising perspectives,” *Frontiers of Medicine*, vol. 6, p. 132, 2019.
- [2] U. Abram and R. Alberto, “Technetium and rhenium: coordination chemistry and nuclear medical applications,” *Journal of the Brazilian Chemical Society*, vol. 17, no. 8, pp. 1486–1500, 2006.
- [3] C. C. Konkankit, S. C. Marker, K. M. Knopf, and J. J. Wilson, “Anticancer activity of complexes of the third row transition metals, rhenium, osmium, and iridium,” *Dalton Transactions*, vol. 47, no. 30, pp. 9934–9974, 2018.
- [4] K. T. Savjani, A. K. Gajjar, and J. K. Savjani, “Drug solubility: importance and enhancement techniques,” *ISRN Pharmaceuticals*, vol. 201210 pages, Article ID 195727, 2012.
- [5] C. Giammei, T. Balber, K. Bencurova et al., “Sorbitol as a polar pharmacological modifier to enhance the hydrophilicity of Tc-99m-tricarbonyl-based radiopharmaceuticals,” *Molecules*, vol. 25, 2020.
- [6] V. L. Gantsho, M. Dotou, M. Jakubaszek et al., “Synthesis, characterization, kinetic investigation and biological evaluation of Re(I) di- and tricarbonyl complexes with tertiary phosphine ligands,” *Dalton Transactions*, vol. 49, no. 1, pp. 35–46, 2020.
- [7] K. Römhild, C. A. Fischer, and T. L. Mindt, “Glycated 99m Tc-tricarbonyl-labeled peptide conjugates for tumor targeting by “click-to-chelate”,” *ChemMedChem*, vol. 12, no. 1, pp. 66–74, 2017.
- [8] S. N. Britvin and A. Lotnyk, “Water-soluble phosphine capable of dissolving elemental gold: the missing link between 1,3,5-triaza-7-phosphaadamantane (PTA) and verkade’s ephemeral ligand,” *Journal Of the American Chemical Society*, vol. 137, no. 16, pp. 5526–5535, 2015.
- [9] L. G. Andrew, D. Phillips, A. Romerosa, F. Vizza, and M. Peruzzini, “Coordination chemistry of 1,3,5-triaza-7-phosphaadamantane (PTA): transition metal complexes and related catalytic, medicinal and photoluminescent applications,” *Coordination Chemistry Reviews*, vol. 248, pp. 955–993, 2004.
- [10] A. Guerriero and L. Gonsalvi, “From traditional PTA to novel CAP: a comparison between two adamantane cage-type aminophosphines,” *Inorganica Chimica Acta*, vol. 518, 2021.
- [11] A. E. Miroslavov, S. N. Britvin, H. Braband et al., “Water-soluble carbonyl complexes of 99Tc(I) and Re(I) with adamantane-cage aminophosphines PTA and CAP,” *Journal of Organometallic Chemistry*, vol. 896, pp. 83–89, 2019.
- [12] T. Scattolin, V. A. Voloshkin, E. Martynova et al., “Synthesis and catalytic activity of palladium complexes bearing N-heterocyclic carbenes (NHCs) and 1,4,7-triaza-9-phosphatricyclo[5.3.2.1]tridecane (CAP) ligands,” *Dalton Transactions*, vol. 50, no. 27, pp. 9491–9499, 2021.
- [13] A. Guerriero, M. Peruzzini, and L. Gonsalvi, “Coordination chemistry of 1,3,5-triaza-7-phosphatricyclo[3.3.1.1]decane (PTA) and derivatives. Part III. Variations on a theme: novel architectures, materials and applications,” *Coordination Chemistry Reviews*, vol. 355, pp. 328–361, 2018.

- [14] J. Bravo, S. Bolaño, L. Gonsalvi, and M. Peruzzini, "Coordination chemistry of 1,3,5-triaza-7-phosphaadamantane (PTA) and derivatives. Part II. The quest for tailored ligands, complexes and related applications," *Coordination Chemistry Reviews*, vol. 254, no. 5-6, pp. 555-607, 2010.
- [15] B. S. Murray, M. V. Babak, C. G. Hartinger, and P. J. Dyson, "The development of RAPTA compounds for the treatment of tumors," *Coordination Chemistry Reviews*, vol. 306, pp. 86-114, 2016.
- [16] F. Scalambra, P. Lorenzo-Luis, I. de los Ríos, and A. Romerosa, "New findings in metal complexes with anti-proliferative activity containing 1,3,5-triaza-7-phosphaadamantane (PTA) and derivative ligands," *European Journal of Inorganic Chemistry*, vol. 2019, no. 11-12, pp. 1529-1538, Article ID 201801426, 2019.
- [17] P. Sgarbossa, U. Sliwinski-Hill, M. F. C. Guedes da Ilva et al., "Pentafluorophenyl platinum(II) complexes of, 3907 of PTA and its N-allyl and N-benzyl derivatives: synthesis, characterization and biological activity," *Materials*, vol. 12, no. 23, 2019.
- [18] A. F. Alshamrani, T. J. Prior, B. P. Burke et al., "Water-Soluble rhenium phosphine complexes incorporating the  $\text{Ph}_2\text{C}(\text{X})$  motif ( $\text{X} = \text{O}, \text{NH}$ ): structural and cytotoxicity studies," *Inorganic Chemistry*, vol. 59, no. 4, pp. 2367-2378, 2020.
- [19] S. Bolaño, L. Gonsalvi, P. Barbaro et al., "Synthesis, characterization, protonation studies and X-ray crystal structure of  $\text{ReH}_5(\text{PPh}_3)_2(\text{PTA})$  (PTA=1,3,5-triaza-7-phosphaadamantane)," *Journal Of Organometallic Chemistry*, vol. 691, no. 4, pp. 629-637, 2006.
- [20] J. K. Bordoloi, D. Berry, I. U. Khan et al., "Technetium-99m and rhenium-188 complexes with one and two pendant bisphosphonate groups for imaging arterial calcification," *Dalton Transactions*, vol. 44, no. 11, pp. 4963-4975, 2015.
- [21] E. Maccaroni, H. Dong, O. Blacque, H. W. Schmalle, C. M. Frech, and H. Berke, "Water soluble phosphine rhenium complexes," *Journal Of Organometallic Chemistry*, vol. 695, no. 4, pp. 487-494, 2010.
- [22] A. Marchi, E. Marchesi, L. Marvelli, P. Bergamini, V. Bertolasi, and V. Ferretti, "New water-soluble rhenium complexes with 1,3,5-triaza-7-phosphaadamantane (PTA)—X-ray crystal structures of  $[\text{ReNCl}_2(\text{PTA})_3]$ ,  $[\text{ReO}_2\text{Cl}(\text{PTA})_3]$ ,  $[\text{ReCl}_3(\text{PTA})_2(\text{PPh}_3)]$ , and  $[\text{Re}_2\text{N}_2\text{Cl}_3(\text{Et}_2\text{dtc})(\text{PTA})_4]$ ," *European Journal of Inorganic Chemistry*, vol. 2008, no. 17, 2679 pages, Article ID 200800114, 2008.
- [23] L. M. D. R. S. Martins, E. C. B. A. Alegria, P. Smoleński, M. L. Kuznetsov, and A. J. L. Pombeiro, "Oxorhenium complexes bearing the water-soluble tris(pyrazol-1-yl)methanesulfonate, 1,3,5-triaza-7-phosphaadamantane, or related ligands, as catalysts for Baeyer-Villiger oxidation of ketones," *Inorganic Chemistry*, vol. 52, no. 8, pp. 4534-4546, 2013.
- [24] L. Marvelli, P. Bergamini, A. Marchi, G. Bersani, V. Ferretti, and V. Bertolasi, "Direct formation of new water soluble Re and Tc complexes containing PTA (1,3,5-triaza-7-phosphaadamantane) from their permetallated salts. Reactivity and X-ray crystal structures," *Inorganica Chimica Acta*, vol. 470, pp. 352-359, 2018.
- [25] X. Shan, A. Ellern, and J. H. Espenson, "Methyl transfer from rhenium to coordinated thiolate groups," *Angewandte Chemie*, vol. 114, no. 20, pp. 3961-3963, 2002.
- [26] P. Smoleński and A. J. L. Pombeiro, "Water-soluble and stable dinitrogen phosphine complexes  $\text{trans}[\text{ReCl}(\text{N}_2)(\text{PTA-H})_n(\text{PTA})_{4-n}]^+ (n=0-4)$ , the first with 1,3,5-triaza-7-phosphaadamantane," *Dalton Transactions*, vol. 1, no. 1, pp. 87-91, 2008.
- [27] R. Schibli, K. V. Katti, W. A. Volkert, and C. L. Barnes, "Novel coordination behavior of  $\text{fac}[\text{ReBr}_3(\text{CO})_3]^{2-}$  with 1,3,5-triaza-7-phosphaadamantane (PTA). Systematic investigation on stepwise replacement of the halides by PTA ligand. Phase transfer studies and X-ray crystal structure of  $[\text{NEt}_4][\text{ReBr}_2(\text{PTA})(\text{CO})_3]$ ,  $[\text{ReBr}(\text{PTA})_2(\text{CO})_3]$ , and  $[\text{Re}(\text{PTA})_3(\text{CO})_3]\text{PF}_6$ ," *Inorganic Chemistry*, vol. 37, no. 20, pp. 5306-5312, 1998.
- [28] I. Chakraborty, S. J. Carrington, G. Roseman, and P. K. Mascharak, "Synthesis, structures, and CO release capacity of a family of water-soluble PhotoCORMs: assessment of the biocompatibility and their phototoxicity toward human breast cancer cells," *Inorganic Chemistry*, vol. 56, no. 3, pp. 1534-1545, 2017.
- [29] R. S. Herrick, C. J. Ziegler, S. Sripathongnak et al., "Preparation and characterization of rhenium (I) tricarbonyl dithiocarbamate compounds;  $\text{Re}(\text{CO})_3(\text{S}_2\text{CNMe}_2)(\text{L})$ ," *Journal of Organometallic Chemistry*, vol. 694, no. 24, pp. 3929-3934, 2009.
- [30] A. Manicum, O. Alexander, M. Schutte-Smith, and H. G. Visser, "Synthesis, characterization and substitution reactions of  $\text{fac}[\text{Re}(\text{O},\text{O}'\text{-bid})(\text{CO})_3(\text{P})]$  complexes, using the "2 + 1" mixed ligand model," *Journal Of Molecular Structure*, vol. 1209, 2020.
- [31] A. Manicum, M. Schutte-Smith, O. T. Alexander, L. Twigg, A. Roodt, and H. G. Visser, "First kinetic data of the CO substitution in  $\text{fac}[\text{Re}(\text{L},\text{L}'\text{-Bid})(\text{CO})_3(\text{X})]$  complexes ( $\text{L},\text{L}'\text{-Bid} = \text{acetylacetonate}$  or  $\text{tropolonate}$ ) by tertiary phosphines PTA and  $\text{PPh}_3$ : synthesis and crystal structures of water-soluble rhenium(I) tri- and dicarbonyl complexes with 1,3,5-triaza-7-phosphaadamantane (PTA)," *Inorganic Chemistry Communications*, vol. 101, pp. 93-98, 2019.
- [32] S. C. Marker, S. N. MacMillan, W. R. Zipfel, Z. Li, P. C. Ford, and J. J. Wilson, "Photoactivated in vitro anticancer activity of rhenium(I) tricarbonyl complexes bearing water-soluble phosphines," *Inorganic Chemistry*, vol. 57, no. 3, pp. 1311-1331, 2018.
- [33] R. Kia and A. Kalaghchi, "Structural, non-covalent interaction, and natural bond orbital studies on bromido-tricarbonyl rhenium(I) complexes bearing alkyl-substituted 1,4-diazabutadiene (DAB) ligands," *Crystals*, vol. 10, no. 4, pp. 267-279, 2020.
- [34] R. Kia, S. Mahmoudi, and P. R. Raithby, "New rhenium-tricarbonyl complexes bearing halogen-substituted bidentate ligands: structural, computational and Hirshfeld surfaces studies," *CrystEngComm*, vol. 21, no. 1, pp. 77-93, 2019.
- [35] W. F. Mark-Lee, Y. Y. Chong, and M. B. Kassim, "Supramolecular structures of rhenium(I) complexes mediated by ligand planarity via the interplay of substituents," *Acta Crystallographica Section C Structural Chemistry*, vol. 74, no. 9, pp. 997-1006, 2018.
- [36] M. B. Ismail, I. N. Booysen, and M. P. Akerman, "Coordination susceptibilities of cinnamaldehyde and cuminaldehyde derived Schiff bases towards the  $\text{fac}[\text{Re}(\text{CO})_3]^+$  core: formation, computational and DNA interaction studies," *Inorganica Chimica Acta*, vol. 477, pp. 257-269, 2018.
- [37] V. S. Christopher Krauss, V. Smith, C. Krauss et al., "The effect of novel rhenium compounds on lymphosarcoma, PC-3 prostate and myeloid leukemia cancer cell lines and an investigation on the DNA binding properties of one of these compounds through electronic spectroscopy," *Journal of Bioprocessing & Biotechniques*, vol. 04, no. 1, pp. 141-212, 2013.

- [38] F. H. Allen, C. A. Baalham, J. P. M. Lommerse, and P. R. Raithby, "Carbonyl-carbonyl interactions can be competitive with hydrogen bonds," *Acta Crystallographica Section B Structural Science*, vol. 54, no. 3, pp. 320–329, 1998.
- [39] J. Echeverría, "Intermolecular carbonyl-carbonyl interactions in transition-metal complexes," *Inorganic Chemistry*, vol. 57, no. 9, pp. 5429–5437, 2018.
- [40] J. Echeverría, "The  $n\pi^*$  interaction in metal complexes," *Chemical Communications*, vol. 54, no. 24, pp. 3061–3064, 2018.
- [41] A. Guerriero, W. Oberhauser, T. Riedel, M. Peruzzini, P. J. Dyson, and L. Gonsalvi, "New class of half-sandwich ruthenium(II) arene complexes bearing the water-soluble CAP ligand as an in vitro anticancer agent," *Inorganic Chemistry*, vol. 56, no. 10, pp. 5514–5518, 2017.
- [42] R. Alberto, A. Egli, U. Abram, K. Hegetschweiler, V. Gramlich, and P. A. Schubiger, "Synthesis and reactivity of  $[\text{NEt}_4]_2[\text{ReBr}_3(\text{CO})_3]$ . Formation and structural characterization of the clusters  $[\text{NEt}_4][\text{Re}_3(\mu_3\text{-OH})(\mu\text{-OH})_3(\text{CO})_9]$  and  $[\text{NEt}_4][\text{Re}_2(\mu\text{-OH})_3(\text{CO})_6]$  by alkaline titration," *Journal of the Chemical Society Dalton Transactions*, vol. 19, pp. 2815–2820, 1994.
- [43] C. Triantis, A. Shegani, C. Kiritsis et al., "Dicarbonyl cis- $[\text{M}(\text{CO})_2(\text{N}, \text{O})(\text{C})(\text{P})]$  ( $\text{M} = \text{Re}, 99\text{mTc}$ ) complexes with a new  $[2+1+1]$  donor atom combination," *Inorganic Chemistry*, vol. 57, no. 14, pp. 8354–8363, 2018.
- [44] R. Schibli, R. La Bella, R. Alberto et al., "Influence of the denticity of ligand systems on the in vitro and in vivo behavior of  $99\text{mTc}(\text{I})$ -tricarbonyl complexes: a hint for the future functionalization of biomolecules," *Bioconjugate Chemistry*, vol. 11, no. 3, pp. 345–351, 2000.
- [45] T. W. Rigaku, *Crystal Clear*, Rigaku/MSI Inc, Woodlands, TX, USA, 2005.
- [46] G. M. Sheldrick, "A short history of SHELX," *Acta Crystallographica Section A Foundations of Crystallography*, vol. 64, no. 1, pp. 112–122, 2008.
- [47] G. M. Sheldrick, "Crystal structure refinement with SHELXL," *Acta Crystallographica Section C Structural Chemistry*, vol. 71, no. 1, pp. 3–8, 2015.
- [48] V. Diamond, *Crystal and Molecular Structure Visualization, Crystal Impact*, Vol. 30, Rathausgasse, Bonn, Germany, 1999.
- [49] P. R. Spackman, M. J. Turner, J. J. McKinnon, S. K. Wolff, D. J. Grimwood, and D. Jayatilaka, "CrystalExplorer: a program for Hirshfeld surface analysis, visualization and quantitative analysis of molecular crystals," *Journal of Applied Crystallography*, vol. 54, no. 3, pp. 1006–1011, 2021.
- [50] J. J. McKinnon, M. A. Spackman, and A. S. Mitchell, "Novel tools for visualizing and exploring intermolecular interactions in molecular crystals," *Acta Crystallographica Section B Structural Science*, vol. 60, no. 6, pp. 627–668, 2004.
- [51] D. Papagiannopoulou, C. Triantis, V. Vassileiadis et al., "Synthesis, structural characterization and radiochemistry of di- and tricarbonyl  $\text{Re}(\text{I})$  and  $99\text{mTc}(\text{I})$  complexes with 8-hydroxyquinoline or 8-mercaptoquinoline and triphenylphosphine," *Polyhedron*, vol. 68, pp. 46–52, 2014.
- [52] P. Kyprianidou, C. Tsoukalas, A. Chiotellis et al., "First example of well-characterized  $\text{Re}$  and  $99\text{mTc}$  tricarbonyl complexes of ciprofloxacin and norfloxacin in the development of infection-specific imaging agents," *Inorganica Chimica Acta*, vol. 370, no. 1, pp. 236–242, 2011.
- [53] O. Karagiorgou, G. Patsis, M. Pelecanou et al., "(S)-(2-(2'-Pyridyl)ethyl)cysteamine and (S)-(2-(2'-Pyridyl)ethyl)-d,l-homocysteine as ligands for the "fac- $[\text{M}(\text{CO})_3]^+$ " ( $\text{M} = \text{Re}, 99\text{mTc}$ ) core," *Inorganic Chemistry*, vol. 44, no. 12, pp. 4118–4120, 2005.
- [54] A. Lazopoulos, C. Triantis, A. Shegani et al., "Effective labeling of amine pharmacophores through the employment of 2,3-pyrazinedicarboxylic anhydride and the generation of fac- $[\text{M}(\text{CO})_3(\text{PyA})\text{P}]$  and cis-trans- $[\text{M}(\text{CO})_2(\text{PyA})\text{P}_2]$  complexes ( $\text{PyA} = \text{pyrazine-2-carboxylate}$ ,  $\text{P} = \text{phosphine}$ ,  $\text{M} = \text{Re}, 99\text{mTc}$ )," *Inorganic Chemistry*, vol. 60, no. 23, pp. 17509–17516, 2021.
- [55] Z. Ozer and S. Ozkar, "C-13-and P-31-NMR study of tetra-carbonylbis(diphenylphosphino)alkanametal(0) complexes of the group 6 elements," *Turkish Journal of Chemistry*, vol. 23, no. 1, pp. 9–14, 1999.
- [56] S. N. Britvin, A. M. Romyantsev, A. E. Zobnina, and M. V. Padkina, "Between adamantane and atrane: intrabridgehead interactions in the cage-like phosphane related to a novel tris(homoadamantane) ring system," *Chemistry—A European Journal*, vol. 22, no. 40, 2016.
- [57] R. Kia, T. Taghavi, and P. R. Raithby, "Supramolecular assembly through intermolecular  $n\pi^*$  interactions through a coordinated perhenate formed via superoxidation of  $\text{Re}(\text{I})$  to  $\text{Re}(\text{VII})$  in the formation of substituted  $\text{Re}(\text{CO})_3$  complexes bearing Diimine ligands," *CrystEngComm*, vol. 22, no. 39, pp. 6448–6452, 2020.